

Global Survey of Precipitation Properties Observed during Tropical Cyclogenesis and Their Differences Compared to Nondeveloping Disturbances

JONATHAN ZAWISLAK

Cooperative Institute for Marine and Atmospheric Studies, University of Miami, and NOAA/Atlantic Oceanographic and Meteorological Laboratory/Hurricane Research Division, Miami, Florida

(Manuscript received 26 November 2018, in final form 4 November 2019)

ABSTRACT

This study evaluates precipitation properties involved in tropical cyclogenesis by analyzing a multiyear, global database of passive microwave overpasses of the pregenesis stage of developing disturbances and nondeveloping disturbances. Precipitation statistics are quantified using brightness temperature proxies from the 85–91-GHz channels of multiple spaceborne sensors, as well as retrieved rain rates. Proxies focus on the overall raining area, areal coverage of deep convection, and the proximity of precipitation to the disturbance center. Of interest are the differences in those proxies for developing versus nondeveloping disturbances, how the properties evolve during the pregenesis stage, and how they differ globally. The results indicate that, of all of the proxies examined, the total raining area and rain volume near the circulation center are the most useful precipitation-related predictors for genesis. The areal coverage of deep convection also differentiates developing from nondeveloping disturbances and, similar to the total raining area, generally also increases during the pregenesis stage, particularly within a day of genesis. As the threshold convective intensity is increased, pregenesis cases are less distinguishable from nondeveloping disturbances. Relative to the western Pacific and Indian Oceans, the Atlantic and eastern North Pacific Oceans have less precipitation and deep convection observed during genesis and the smallest differences between developing and nondeveloping disturbances. This suggests that the total raining area and areal coverage of deep convection associated with tropical disturbances are better predictors of tropical cyclogenesis fate in the Pacific and Indian Oceans than in the Atlantic and eastern North Pacific.

1. Introduction

An accurate prediction of tropical cyclogenesis (i.e., TC genesis) requires an understanding of both the necessary conditions for tropical cyclone (TC) formation on the large scale and the precipitation organization on the mesoscale that favors the development of a TC-strength vortex in the presence of those large-scale conditions. It is likely that the thermodynamic and kinematic structure of the disturbance is closely coupled with the precipitation processes, such that when the large-scale conditions are favorable for TC genesis, the development fate of tropical disturbances is likely tied to how precipitation organizes within the disturbance, and subsequently how the kinematic and thermodynamic structures respond to that precipitation.

Previous literature has typically presented TC genesis as following either a “top down” or “bottom up” pathway.

In the top-down pathway, TC formation generally involves intensification of a midtropospheric mesoscale cyclonic vortex (MCV) originating in the stratiform rain region of a mesoscale convective system (MCS); in the bottom-up pathway, genesis emerges from the aggregation, or axisymmetrization, of individual deep, vortical convective towers [vortical hot tower (VHT)] within an already cyclonic vorticity-rich environment (Hendricks et al. 2004; Montgomery et al. 2006). It is more likely, however, that aspects of both pathways contribute such that multiple precipitation modes (shallow, moderately deep, and deep convection, as well as stratiform rain) are responsible for genesis (Wang 2012; Fritz et al. 2016). This has been supported by a wealth of evidence from observational case studies that have linked precipitation to key kinematic and thermodynamic processes occurring during TC genesis (e.g., Ritchie and Holland 1997; Simpson et al. 1997; Raymond et al. 2011; Raymond and López Carrillo 2011; Davis and Ahijevych 2012; Komaromi 2013; Zawislak and Zipser 2014a,b). These case studies support a genesis pathway

Corresponding author: Jonathan Zawislak, jonathan.zawislak@noaa.gov

in which an organized midtropospheric (i.e., $\sim 2\text{--}5$ km) circulation develops and the tropospheric stability increases (the upper troposphere warms and the lower troposphere cools)—likely reflecting dominant stratiform rain processes. More important, the middle troposphere is preconditioned as it moistens due to detrainment from moderately deep cumulus congestus (Wang 2012, 2014). In an environment preconditioned by a coherent midtropospheric circulation and a moist, near-saturated troposphere, contributions from deep convection to development are favored, a more bottom-heavy mass flux profile is observed, and spinup in the low troposphere is preferred (Nolan 2007; Raymond and Sessions 2007; Raymond et al. 2011; Raymond and López Carrillo 2011).

One of the few studies to examine multiyear composites of precipitation properties during TC formation, Fritz et al. (2016) analyzed Tropical Rainfall Measuring Mission (TRMM) Precipitation Radar (PR) satellite data from 1998 to 2010 to examine individual contributions from stratiform rain, and shallow, moderately deep, and deep convection, to genesis. They concluded that genesis involves the collective contributions from these different precipitation types. However, the relatively large areal coverage of moderately deep convection and stratiform rain made these precipitation types the largest contributors to precipitation involved in genesis. Deep convection had the largest contribution to pixel rain rate, but its areal coverage was far exceeded by the other precipitation types they defined. Although it does not extend over the entire troposphere, they surmise that cumulus congestus favors a transition to deep convection as midlevel congestus clouds moisten the midtroposphere through detrainment (Wang 2014). The present study will complement Fritz et al. (2016) by extending the multiyear analysis to proxies from passive microwave (PMW) satellite data, and it will go further by comparing precipitation properties of developing tropical disturbances to nondeveloping disturbances.

PMW sensor data has been used more extensively in studies of precipitation properties in mature TCs (e.g., Alvey et al. 2015; Tao and Jiang 2015; Tao et al. 2017), but fewer studies have used PMW data to investigate precipitation properties of tropical disturbances prior to TC genesis. Leppert et al. (2013a,b) combine PMW data from the TRMM Microwave Imager (TMI) with data from the TRMM Lightning Imaging Sensor and a merged infrared (IR) satellite dataset to composite statistics for developing and nondeveloping easterly waves in the Atlantic Ocean and eastern North Pacific Ocean. They conclude that the coverage of precipitation and convection may be more important to tropical cyclogenesis than the overall intensity of convection, as it most differentiates the developing

versus nondeveloping easterly waves. This conclusion is verified in case studies shown in Zawislak and Zipser (2014b), a study that serves as the precedent for the method used here.

Wang (2018) composited IR brightness temperature data during the genesis stage for over 150 developing Atlantic Ocean TCs between 1989 and 2010. They found that both convective intensity and the convective frequency (area) increased within the inner pouch region, and that convection appeared to “move” toward the pouch center as the genesis time neared. These findings led to the suggestion that the radial gradient of diabatic heating due to organized convection near the pouch center is a key factor in TC genesis. One of their important conclusions was that the composite mean instead represents a probability of occurrence of convection, and that individual storms likely vary in number of “convective peaks”, convective intensity, area, and duration. Driven by differences in the environmental characteristics (e.g., humidity, vertical shear, and low-level convergence), they identified three distinct spatial patterns of convection: one where a large convective system is displaced $4^{\circ}\text{--}5^{\circ}$ east of the pouch center (they classified as “cluster 1”), another where the convection is displaced south and is less symmetric about the pouch (“cluster 3”), and a third that exhibits a convective system that is weaker and smaller than “cluster 1”, but is more symmetric about the pouch center (“cluster 2”).

This study contributes toward a global survey of the precipitation characteristics associated with developing and nondeveloping tropical disturbances, with a focus on identifying the distinguishing properties of those disturbances that eventually develop into TCs. It builds on previous case studies (Zawislak and Zipser 2014a,b) by examining whether the conclusions drawn from those individual examples are robust when analyzed for a larger sample, while also complimenting and verifying results from studies that use other multiyear satellite datasets (Leppert et al. 2013a,b; Fritz et al. 2016; Wang 2018) to analyze precipitation properties in TC genesis. While these previous studies limit their analysis to the Atlantic and eastern North Pacific basins, this study extends the investigation to other TC-prone basins globally. Characteristics of precipitation involved in tropical cyclogenesis will be compared and contrasted in the different ocean basins. A unique compilation of PMW satellite overpasses, subset for developing (pregenesis stage) and nondeveloping disturbances, is used in this study (described in detail in section 2) that easily facilitates composite analyses over multiple years of cases in all basins. The following questions will be evaluated using both PMW data and retrieved rain rates:

- 1) What precipitation properties most distinguish developing tropical disturbances from nondeveloping disturbances?
- 2) How do the precipitation properties of developing versus nondeveloping tropical disturbances vary between different ocean basins?
- 3) How do various precipitation properties evolve both spatially and temporally during the pregenesis stage of developing disturbances?

2. Dataset descriptions and methodology

a. Track methodology

Precipitation properties are quantified using a unique accumulation of overpasses of the pregenesis stage of developing TCs and nondeveloping tropical disturbances from multiple satellite-borne PMW imagers. The overpasses are a subset of the broader Tropical Cyclone–Passive Microwave (TC-PMW) dataset [used previously by [Alvey et al. \(2015\)](#) for developed TCs], which consists of overpass statistics during all stages of the TC life cycle. Best-track information from National Hurricane Center (NHC) and Joint Typhoon Warning Center (JTWC) serves as the source for both developing and nondeveloping disturbance center locations for overpasses in the TC-PMW, and provides important estimates on the intensity of the disturbance, such as the maximum sustained wind speed and minimum sea level pressure.¹

A pregenesis track consists of the “invest” portion of the best track of a disturbance prior to its initial designation as a tropical depression (TD), and is typically classified as a wave, disturbance, or low. The genesis time is defined as the time of the first classification in the best track as a TD or stronger. An invest designation is given to disturbances that have the potential to undergo genesis so that specialized datasets and model guidance are enabled. An invest does not always develop into a TC, and therefore invests that do not develop are classified as the nondeveloping sample. In the cases of disturbances that develop, later weaken below TD strength, and subsequently redevelop (and thus have multiple genesis times), the later genesis periods are not included in the statistics.

The TC-PMW encompasses all developed (i.e., tropical depression or stronger) TCs globally between 1998

TABLE 1. Number of developing (DEV; with pregenesis tracks available) and nondeveloping (NON) cases in each basin, as well as the total.

	AL	EP	CP	WP	NIO	SH	Total
DEV	214	223	23	317	55	232	1064
NON	209	132	51	359	81	283	1115

and 2015. However, in the basins under NHC responsibility [North Atlantic (AL), eastern North Pacific (EP), and central North Pacific (CP)], the TC-PMW consists of only 13 years (2003–15) of satellite overpasses of pregenesis and nondeveloping disturbances. For basins under the purview of JTWC [northwestern Pacific (WP), northern Indian Ocean (NIO), and Southern Hemisphere (SH)], there are 12 years (2004–15) of developing disturbances with pregenesis tracks available, and 7 years (2009–15) of nondeveloping disturbances. The number of developing (with pregenesis tracks) and nondeveloping disturbances available in each basin is provided in [Table 1](#). There is almost an equal number of contributing developing (1064) and nondeveloping (1115) disturbances in the combined global dataset. An important caveat in the JTWC basins is that the duration of the pregenesis invest tracks tend to be consistently shorter than in the AL and EP/CP, so small sample sizes become an issue more than 3 days before genesis. Though statistics will be shown for each basin separately in [section 4](#), note that distributions that consist of all basins composited together will have greater contributions from the AL and EP/CP.

The use of invest tracks in this study differs from many previous studies on TC genesis. For example, some previous studies have used vorticity maxima in the lower (i.e., 925 and 850 hPa) and middle troposphere (i.e., 700 and 600 hPa) as center positions for pregenesis and nondeveloping tracks (e.g., [Kerns et al. 2008](#); [Kerns and Zipser 2009](#); [Zawislak and Zipser 2010](#)). While such a method will certainly produce a larger case sample, a larger sample does not necessarily guarantee an informative result, particularly for nondeveloping disturbances. Nondeveloping vorticity maxima are more numerous than developing; for example, [Kerns et al. 2008](#) tracked nearly 6 times as many nondeveloping vorticity maxima as developing vorticity maxima (615 nondeveloping vs 97 developing) in the low levels in the AL. A significant portion of those tracks, however, are likely dry, void of rainfall, and/or experiencing substantial vertical wind shear, and are clearly nondevelopers. That the subsets of nondeveloping tracks used in the TC-PMW were designated invests by the various operational centers suggest at least some interest in their potential for future genesis.

¹Note that most of the information contributing toward intensity estimates during the pregenesis stage is from satellite. Even in the Atlantic, where aircraft reconnaissance is routinely available, only a very small portion of the 6-hourly best track has aircraft data contributing toward the location and intensity estimation.

TABLE 2. Properties (frequency, footprint, and years available) of sensors included in the TC-PMW. Note that “End” means that the observation record is available through December 2015, which is the end of the period considered for this study.

Sensor	Frequency (GHz)	Footprint (km × km)	Years available
AMSR-E	89.0	6 × 4	Jun 2002–Oct 2011
AMSR2	89.0	5 × 3	Jul 2012–End
TMI	85.0	7 × 5 (preboost) 8 × 6 (postboost)	Dec 1997–Sep 2014
GMI	89.0	7 × 4	Mar 2014–End
SSM/I-11	85.5	15 × 13	Dec 1991–May 2000
SSM/I-13	85.5	15 × 13	May 1995–Nov 2009
SSM/I-14	85.5	15 × 13	May 1997–Aug 2008
SSM/I-15	85.5	15 × 13	Feb 2000–End
SSMIS-16	91.655	15 × 13	Nov 2005–End
SSMIS-17	91.655	15 × 13	Mar 2008–End
SSMIS-18	91.655	15 × 13	Mar 2010–End
SSMIS-19	91.655	15 × 13	Nov 2014–End

The method in this study is certainly more subjective than using relative vorticity or pouch tracks as it is based on multiple human analysts’ determination of center location (based on available model analysis, satellite, aircraft, and surface wind information) and whether it should or should not be classified as an invest—the methods in making those determinations may differ based on availability of data, from forecast center to forecast center, and even from forecaster to forecaster. However, rather than attempt to account for these differences, instead we simply treat the determination of the center locations and invest status equally for each track position. Despite its subjectivity, having multiple sources of information to classify invests also seems beneficial over a single metric (i.e., pouch, vorticity), especially since it allows for a center to also be determined from, for example, a persistent convective burst that could become the nascent center of the TC. Considering that this track method differs greatly from the other composite genesis studies (e.g., Leppert et al. 2013a,b; Fritz et al. 2016; Wang 2018), there is a unique opportunity here to assess the utility of using invests as an alternative to pouch or relative vorticity tracking.

b. TC-PMW

The TC-PMW includes data from multiple spaceborne PMW sensors, including the TMI; Global Precipitation Measuring Mission (GPM) Microwave Imager (GMI); Advanced Microwave Scanning Radiometer for Earth Observing System (AMSR-E); Global Change Observation Mission-Water (GCOM-W) Advanced Microwave Scanning Radiometer-2 (AMSR2); Special Sensor Microwave Imager (SSM/I) on board the Defense Meteorological Satellite Program *F11*, *F13*, *F14*, and *F15*; and Special Sensor Microwave Imager/Sounder (SSMIS) on board *F16*, *F17*, *F18*, and *F19*. Table 2 lists

the dates of availability of these different sensors, the microwave frequencies used in this study, and the footprints at those frequencies. TMI data are from the level-1, collocated (i.e., measurements from all TRMM instruments on a common grid) dataset of the version-7 TRMM cloud and precipitation feature (TCPF) database [described in Liu et al. (2008)]. GMI data are from version 4 of the GPM Precipitation Processing System intercalibrated level-1C (L1C) algorithm (the Algorithm Theoretical Basis Document is available online at https://pps.gsfc.nasa.gov/Documents/L1C_ATBD.pdf) [see Berg et al. (2016) for a description of intercalibration]. AMSR-E data are from the NASA National Snow and Ice Data Center Distributed Active Archive Center L2A Global Swath Spatially-Resampled Brightness temperature dataset (Ashcroft and Wentz 2013), while AMSR2 data are Japan Aerospace Exploratory Agency (JAXA)/GCOM-W level-1R resampled brightness temperatures. AMSR-E and AMSR2 data are not intercalibrated. SSM/I and SSMIS data are from the Colorado State University Fundamental Climate Data Record (FCDR) dataset (Sapiano et al. 2013). FCDR is an intercalibrated dataset that provides physically consistent brightness temperatures between the SSM/I and SSMIS sensors for the purposes of creating a well-documented, long-term archive of SSM/I and SSMIS data suitable for climate applications. Among five intercalibration techniques applied to the data, one includes matching with coincident passes of TMI.

PMW satellite information is supplemented with rain rates from the NASA TRMM 3B42 product, which is a merged PMW-IR rain rate retrieval (Huffman et al. 2007). This product provides gridded, 3-hourly rain rates at 0.25° horizontal resolution globally between latitudes 37°N and 37°S. The limited latitudes available in TRMM 3B42 compared to the PMW overpasses reduce the sample of tracks available for the rain rate

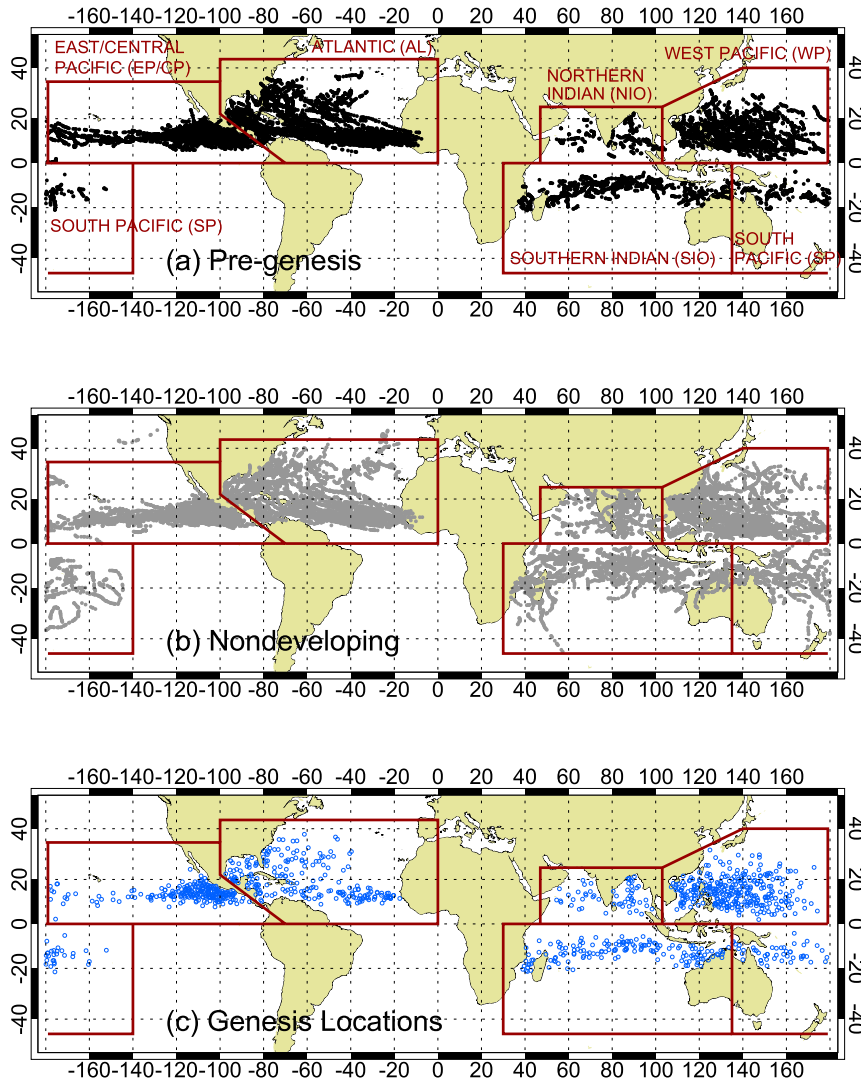


FIG. 1. Disturbance (i.e., invest) center locations for overpasses of (a) the pregenesis stage of developing tropical disturbances (black dots) and (b) nondeveloping tropical disturbances (gray dots), as well as (c) the genesis locations (blue dots) of developing disturbances. Boxes, labeled in (a), outline the approximate boundaries of each basin considered.

statistics compared to the ones for the PMW brightness temperatures.

For the purposes of this study, a PMW overpass is only considered when there is complete coverage of the swath within 3° of the invest center. Figure 1 shows the disturbance center locations in each basin, interpolated to the time of each overpass that meets these criteria. Overpasses of pregenesis and nondeveloping disturbance centers near and over land are included. The close proximity of many genesis locations to land (Fig. 1c) strongly suggests that land does not necessarily impede genesis from occurring. As such, it is important to also consider precipitation occurring in these disturbances despite their close, or overland, proximity. Precipitation

near the disturbance center, regardless of whether it is over land or not, appears to positively contribute to TC genesis in these cases. For the pregenesis evolution analysis, periods will be composited for 24-h periods, rather than 12 hourly, to reduce the influence of the diurnal cycle in the statistics.

Table 3 shows the total number of satellite overpasses of nondeveloping and pregenesis stage disturbances in each basin. Considering the smaller sample sizes of CP cases, CP data will be combined with the EP in the statistical composites. Also, considering the size of the SH basin, the SH disturbances are separated at 135°E longitude [similar to Klotzbach (2014)] into the southern Indian Ocean (SIO) (west of 135°E) and South Pacific

TABLE 3. For each basin, the total number of overpasses (“Total passes”, which includes all stages of the storm, including its postgenesis portion), number of nondeveloping (“NONDEV passes”) and pregenesis (“PRE passes”) overpasses, as well as the number of overpasses with the required complete (100%) data coverage within 3° of the center. The percentage of the total overpasses for each category (NONDEV, PRE, and those with 100% data coverage in 3°) is also shown.

Basin	Total passes	Percent of total passes	NONDEV passes	Percent of total NONDEV passes	PRE passes	Percent of total PRE passes	Passes with 100% data coverage in 3°	Percent of total 100% coverage passes
AL	22 993	22	4651	24.7	4323	32.5	11 426	22.5
EP	19 357	18.5	2792	14.8	3874	29.2	9351	18.4
CP	2628	2.5	785	4.2	588	4.4	1299	2.6
WP	27 976	26.8	4394	23.3	2532	19.1	13 579	26.7
NIO	4689	4.5	1319	7.0	356	2.7	2263	4.4
SH	26 940	25.8	4908	26.0	1603	12.1	12 917	25.4
	104 583	100	18 849	100	13 276	100	50 835	100

(SP) (east of 135°E) (Fig. 1). A minimum in genesis events occurs near this longitude (135°E) and separates common formation regions to the east and west.

This study will use data at PMW frequencies of 85–91 GHz (sensor dependent; Table 2). At 85–91 GHz, the scattering of liquid emission by large size and quantities of ice aloft depresses the brightness temperature in the scene. Following Spencer et al. (1989), polarization corrected temperature (PCT) is used in place of brightness temperature. PCT is a linear combination of the vertical and horizontal polarization brightness temperatures, and removes the ambiguity that exists due to differences in emissivity between land and ocean. Because of its lower emissivity, the ocean appears colder at these higher frequencies, and thus it can be more difficult to differentiate areas of depressed brightness temperature due to deep convection from the ocean background.

Similar to Table 3, Table 4 shows the total number of pregenesis and nondeveloping overpasses, but separated for each PMW sensor. AMSR-E, AMSR2, GMI, TMI, and SSMI(S) (i.e., SSM/I and SSMIS combined) contribute approximately 10%, 6%, 2%, 18%, and 63%, respectively, to the total number of overpasses in both the nondeveloping and pregenesis samples (Table 4). Given that SSMI(S) makes, by far, the largest contribution to the nondeveloping and pregenesis samples, the analyses shown will mostly be reflective of SSMI(S) alone.

All PMW analyses in sections 3 and 4 were replicated individually for the other sensor pairs (AMSR-E/AMSR2 and TMI/GMI) and those results revealed similar conclusions as the combined analyses with all sensors, which provide some support for compositing the differing sensor data together for some metrics.

Care will be taken to account for each sensor’s footprints (Table 2) when interpreting the results. For instance, the distributions of fractional coverage of 85–91-GHz \leq 250 K within 3° of the center (a metric that will be used as a proxy for the total raining area) of all overpasses in the TC-PMW do not differ among sensors (Fig. 2a). As such, data from each sensor is simply composited together for this metric. In contrast, minimum 85–91 GHz, which is the metric used as a proxy for the occurrence of various convective intensities, could be sensor dependent if a threshold PCT below approximately 210 K is applied (Fig. 2b). Above approximately 210 K, the individual sensor distributions are fairly close to one another, and sensor data can reasonably be combined. As the PCT decreases below 210 K (indicative of significant ice scattering and thus more intense convection), the difference between the distributions for the smaller footprint sensors (i.e., high resolution; AMSR-E, AMSR2, GMI, and TMI) and the larger footprint sensors (i.e., low resolution; SSM/I and SSMIS) becomes greater. The PCT at any given percentile is lower for the high-resolution sensors; as such, these sensors are more likely

TABLE 4. As in Table 3, but separated for each sensor (SSM/I and SSMIS are combined).

Sensor	Total Passes	Percent of total passes	NONDEV passes	Percent of total NONDEV passes	PRE passes	Percent of total PRE passes	Passes with 100% data coverage in 3°	Percent of total 100% coverage passes
AMSR-E	10 835	10.4	1955	10.4	1458	11.0	6147	12.1
AMSR2	5067	4.8	1124	6.0	850	6.4	2916	5.7
TMI	20 529	19.6	3317	17.6	2363	17.8	4160	8.2
GMI	1893	1.8	438	2.3	307	2.3	506	1.0
SSMI(S)	66 259	63.4	12 015	63.7	8298	62.5	37 106	73.0
	104 583	100	18 849	100	13 276	100	50 835	100

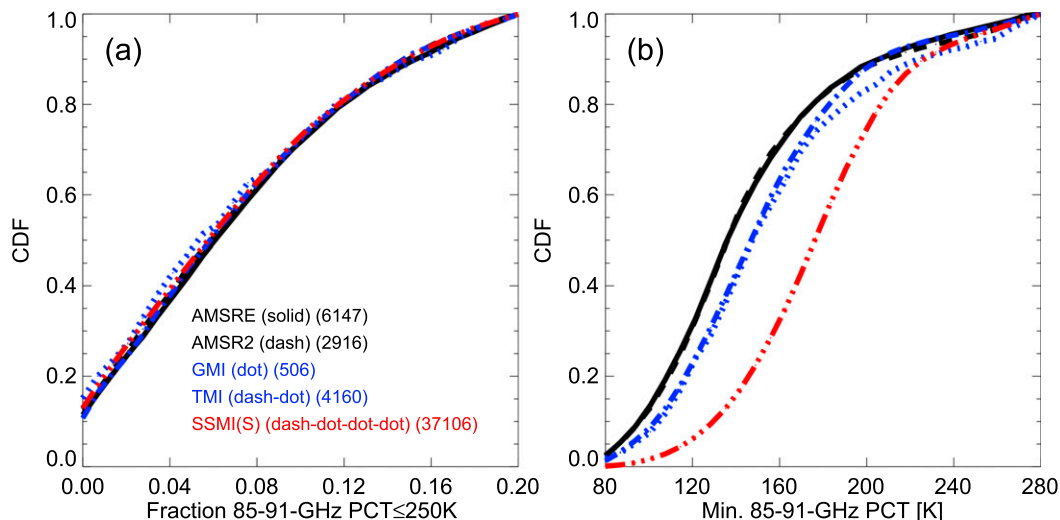


FIG. 2. Cumulative distribution function of (a) the fraction of 85–91-GHz PCT \leq 250 K and (b) minimum 85–91-GHz PCT, within 3° of the center, separated by each PMW sensor (SSM/I and SSMIS are combined). Sample sizes are noted in parentheses in the legend in (a).

to detect smaller-scale, intense convective cores than SSM/I and SSMIS. Therefore, any metric using a threshold PCT below approximately 210 K (related to increasingly more intense convection), sensor-dependent thresholds would need to be applied for compositing.

3. Basin differences between developing and nondeveloping disturbances

a. Total raining area

Figure 3a compares the nondeveloping and pregenesis cumulative distribution functions (CDFs) (hereinafter “distributions”) of the raining fraction within 3° of the disturbance center (where $3B42 \text{ rain rate}^2 > 0.1 \text{ mm h}^{-1}$), which for the purposes of this study serves as a proxy for the total raining (precipitating) area. The pregenesis CDF includes all overpasses of the pregenesis stage, regardless of the number of hours before genesis. While the pregenesis stage raining fractions are significantly larger³ than the raining fractions in nondeveloping disturbances in each basin, the magnitude of the difference between the pregenesis and nondeveloping distributions varies by basin. The largest difference in raining fraction between

the pregenesis stage and nondeveloping disturbances is in the SP, NIO, SIO, and WP (in that order, from highest to lowest median raining fraction), while the smallest differences are found for the AL and EP/CP. Overall, the AL appears to have the smallest total raining area during the pregenesis stage, while the NIO and SP have the largest. In fact, the pregenesis distribution in the AL is comparable to the nondeveloping distributions in the EP/CP and SP. That the AL exhibits the least difference between the pregenesis and nondeveloping distributions could be interpreted that it is the most difficult basin to predict whether a disturbance will develop or not, based on total raining area alone. While in the NIO and SP, closely followed by the SIO and WP, the total raining area could be a better predictor of the genesis fate as those basins exhibit the greatest difference between developing and nondeveloping disturbances.

Figure 3b is similar to Fig. 3a, except it illustrates the distributions for the fractional coverage of 85–91-GHz PCT \leq 250 K, a PMW proxy for total precipitating (raining) area. Spencer et al. (1989) concluded that PCT of 250–260 K in the 85-GHz channel indicated sufficient ice scattering to produce surface rainfall of at least 1–3 mm h^{-1} . Alvey et al. (2015) classified this threshold as “moderate” precipitation for TC composites from the TC-PMW. Therefore, while this proxy includes precipitation weaker than deep convection, it does threshold precipitation somewhat more intense than the 3B42 analysis in Fig. 3a. Figure 3b indicates that the NIO has the highest areal coverage of rainfall, or moderate precipitation, of any basin during the pregenesis stage, followed by the SP, SIO, WP, EP/CP, and finally the AL

² Retrieved rain rates from 3B42 are considered to be less reliable at weaker intensities ($< 1 \text{ mm h}^{-1}$). A threshold of 0.1 mm h^{-1} is applied, rather than 1 mm h^{-1} , since that high of a threshold would likely be too restrictive at the horizontal resolution of 3B42.

³ In this study, statistical significance testing between distributions uses the Wilcoxon rank sum test and will be assessed at the 99% confidence level.

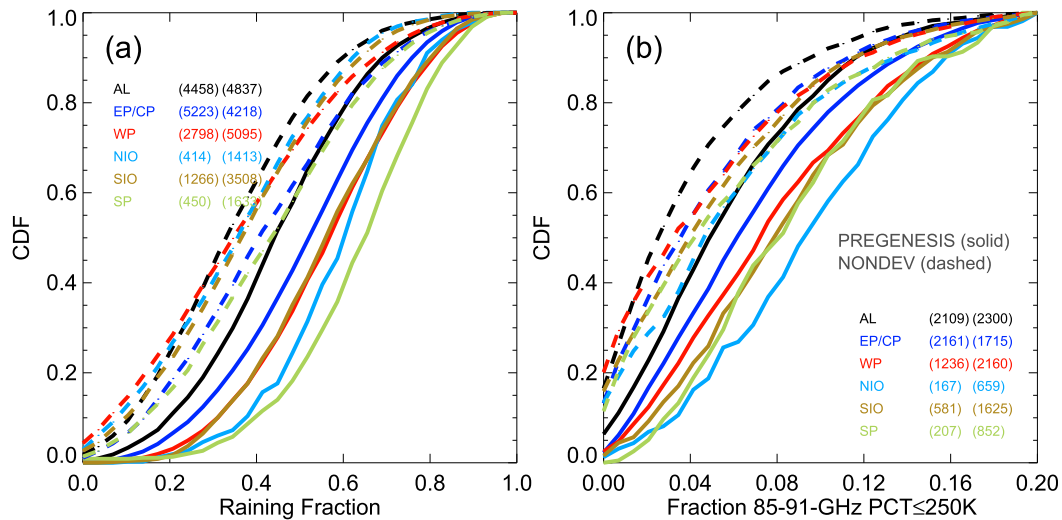


FIG. 3. CDF of (a) raining fraction (3B42 rain rate $> 0.1 \text{ mm h}^{-1}$) and (b) fractional coverage of 85–91-GHz PCT $\leq 250 \text{ K}$ within 3° of the center for the pregenesis stage of developing disturbances (solid) and nondeveloping disturbances (dashed) for the various basins. Sample sizes are noted in the legends, with the pregenesis and nondeveloping sample sizes noted in the left and right sets of parentheses, respectively.

(ordered from highest to lowest median value). Results in this figure, most notably the significant differences between the developing and nondeveloping distributions in each basin, are consistent with the 3B42 raining fraction distributions shown in Fig. 3a.

In addition to differences existing between each basin for the total raining area (Fig. 3), there are also pregenesis and nondeveloping differences between basins for rain rate. Figure 4 shows the distributions of conditional mean rain rate (i.e., computed only for raining pixels in 3B42; rain rate $> 0.1 \text{ mm h}^{-1}$) within 3° of the center for each basin. The mean rain rates follow closely with the total raining area (Fig. 3) as there is not only a significant difference in mean rain rates between developing and nondeveloping distributions in each basin, but also the NIO, WP, SP, and SIO basins (in that order from highest to lowest median conditional mean rain rate) exhibit distinguishably larger mean rain rates than the AL and EP/CP for both pregenesis and nondeveloping cases. In combination, Figs. 3 and 4 strongly suggest that the rain volume, consisting of contributions from rain rate and raining area, is larger in developing disturbances than nondeveloping, and that developing disturbances exhibit less rainfall in the AL and EP/CP than the other basins.

b. Areal coverage of deep convection

Figure 5a differentiates the pregenesis and nondeveloping distributions in each basin for the fractional coverage of “heavy” rain, defined as 3B42 rain rate $\geq 5 \text{ mm h}^{-1}$ within 3° of the center. This metric serves as a proxy for

the areal coverage of deep convection. Although stratiform rain can certainly exceed a rain rate of 5 mm h^{-1} , considering the coarse resolution of 3B42 ($\sim 25 \text{ km}$) this threshold is considered sufficiently intense to be more likely associated with convection (Zawislak and Zipser 2014b also used this threshold). Similar to the raining fraction (Fig. 3a), Fig. 5a indicates that in all basins the fractional coverage of heavy rain (i.e., deep convection)

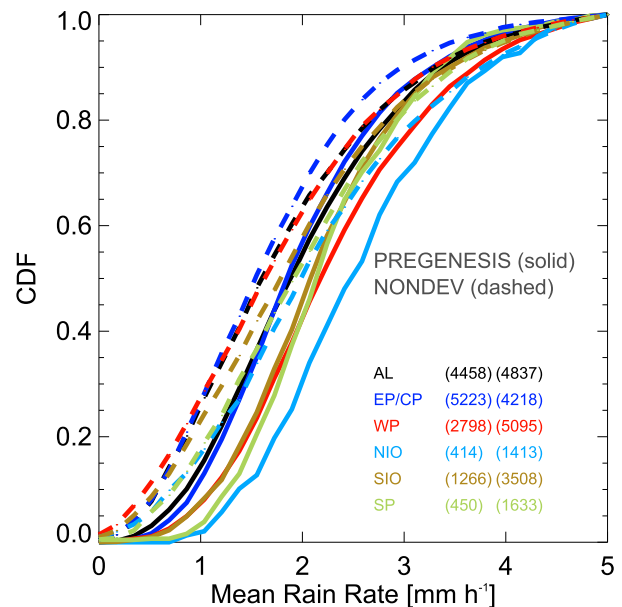


FIG. 4. Similar to Fig. 3a, but for the CDF of the conditional mean 3B42 rain rate.

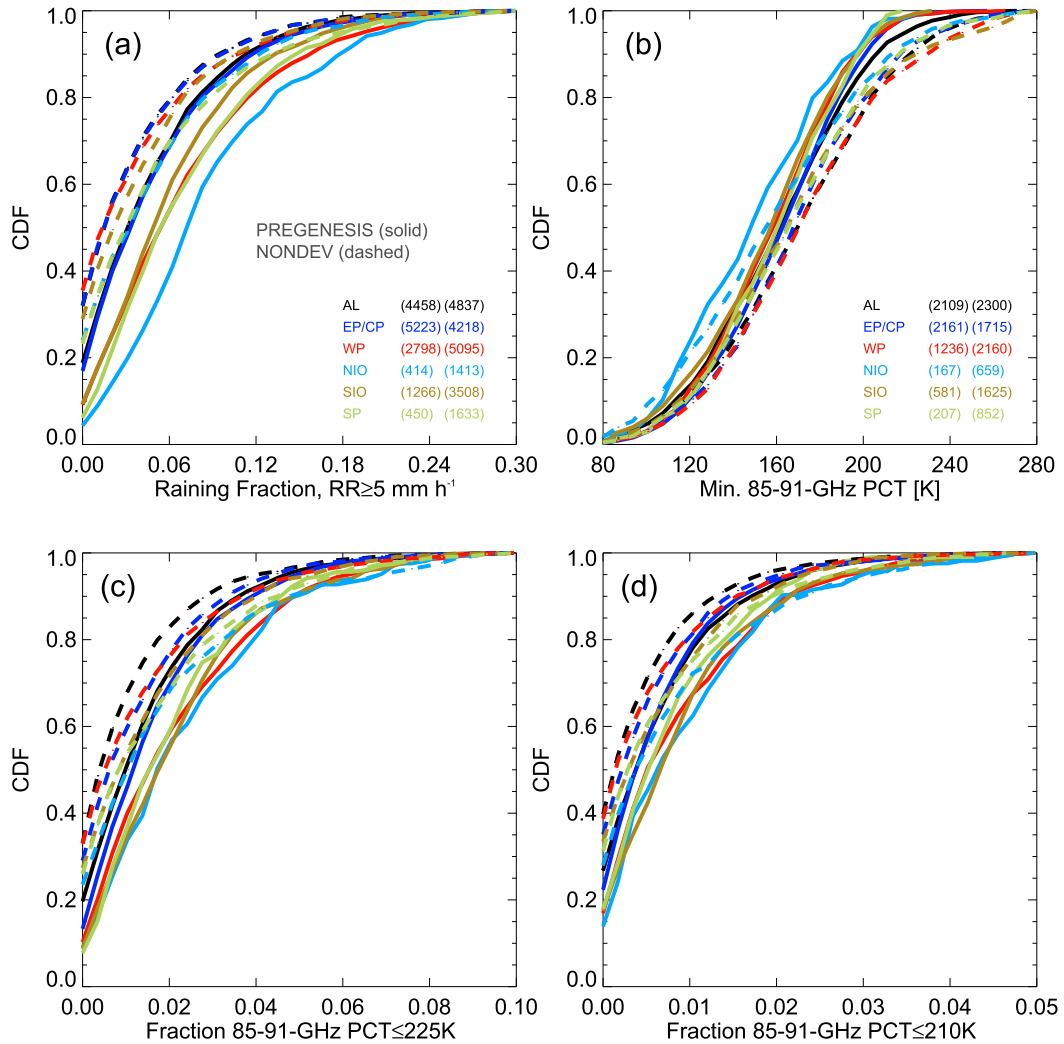


FIG. 5. Similar to Fig. 3, but for the CDF of (a) the fractional coverage of heavy rain (3B42 rain rate $\geq 5 \text{ mm h}^{-1}$), (b) minimum 85–91-GHz PCT, (c) the fractional coverage of 85–91-GHz PCT $\leq 225 \text{ K}$, and (d) the fractional coverage of 85–91-GHz PCT $\leq 210 \text{ K}$. Sample sizes noted in (b) are the same for (c) and (d).

in the pregenesis stage of developing disturbances is significantly greater than in nondeveloping disturbances. Likewise, Fig. 5a suggests that the largest fractional coverage of heavy rain in developing disturbances is in the NIO, WP, SP, and SIO (in order from highest to lowest median values). Like the total raining area (Fig. 3a), the AL and EP/CP have the smallest fractional coverage of heavy rain prior to genesis and exhibit the least difference between the pregenesis and nondeveloping cases. Coverage of heavy rain, however, does appear to more easily differentiate developing from nondeveloping disturbances in the other basins and, similar to the total raining area, could serve as a better predictor of genesis fate in the WP, SIO, SP, and NIO.

Mohr and Zipser (1996) quantified a threshold value of SSM/I 85-GHz PCT $< 225 \text{ K}$ to assess deep convection

associated with an MCS. Considering that the TC-PMW dataset is dominated by SSMI(S), this PCT threshold will be used as one of the PMW proxies for the areal coverage of deep convection. This threshold is similarly applied to all other sensors for the composite in Fig. 5c, which compares the distributions of the areal coverage of deep convection (85–91-GHz PCT $\leq 225 \text{ K}$) within 3° of the center for the pregenesis stage and nondeveloping disturbances in each basin. The distributions indicate that, in all basins, there is significantly greater areal coverage of deep convection in the pregenesis stage than in nondeveloping disturbances. Similar to the 3B42 heavy rain composites (Fig. 5a), the AL and EP/CP have the smallest areal coverage of deep convection of all basins, although in some contrast, the separation between pregenesis and

nondeveloping distributions in the other basins is reduced for the PMW proxy.

Figure 5d shows distributions for 85–91-GHz PCT \leq 210 K, which thresholds somewhat more intense convection than 225 K. Albeit the fractional coverage of 210 K is nearly one-half of 225 K (less than 5% as compared with 10% for 225 K), the figure suggests that the difference between the pregenesis and nondeveloping distributions in almost every basin are somewhat less distinguishable, though still significantly different, than what was observed for the 225 K threshold. Figure 5b, which shows the pregenesis and nondeveloping minimum 85–91-GHz PCT distributions, provides further evidence of this trend. Note that as the minimum PCT observed in an overpass decreases (indicative of more intense convection) below 210 K, the degree of difference between the pregenesis and nondeveloping distributions decreases. This suggests that the occurrence of more intense convection, and likely the areal coverage of that convection, could make it a less useful predictor for separating developing cases; a result consistent with the conclusions from Leppert et al. (2013a,b) and Zawislak and Zipser (2014b). This result does not imply that intense convection is not important to genesis, just that its occurrence does not differentiate it well from nondeveloping cases. In fact, considering how small the 210 K areal fractions are (<5% of the area), even what would appear to be a small increase in fractional coverage could be very influential on the vortex development. One must be cautious of the robustness of these results, however, considering that there are just so few pixels at these low PCTs and that the detection of low PCTs associated with intense convection is very sensitive to the individual PMW sensors. Likewise, this and other conclusions about the “usefulness” as a genesis predictor are based on a composite of cases; certainly comparisons between some individual developing and nondeveloping storms likely deviate from the composite results shown here (e.g., an individual nondeveloping disturbance within this case sample could certainly exhibit consistently greater convective area than other developing cases).

c. Spatial coverage and proximity of precipitation to the center

Figure 6 compares the spatial distribution and fractional occurrence of 85–91-GHz PCT \leq 250 K for the pregenesis stage and nondeveloping disturbances. In this figure, data have been interpolated onto a 13×13 km² resolution grid such that, for compositing purposes, the high-resolution PMW sensors are at a similar resolution as the larger footprint SSMI(S) (Table 2). PMW data have also been rotated relative to the 500-km

average 850–200-hPa (deep layer) vertical wind shear heading [as computed from the 6-hourly National Centers for Environmental Prediction Final (FNL) model analyses], such that shear-relative quadrants [downshear right (DSR), downshear left (DSL), upshear right (USR), and upshear left (USL)] are separated. While the composite in Fig. 6 individualized for each basin is not shown here, similar results were identified in each of the basins. Although the greatest occurrence of precipitation is downshear in both developing and nondeveloping disturbances, the most distinguishing difference is not only the higher occurrence of precipitation during the pregenesis stage, but also the increased azimuthal coverage of precipitation in all quadrants around the center. Perhaps interestingly, though, the peak location of precipitation is not any closer to the center during the pregenesis stage than in nondeveloping disturbances. This suggests that while the close proximity of precipitation to the center (e.g., peak within ~50–150 km) is favorable for genesis to occur, it may not be sufficient alone to develop a TC; the increased coverage of precipitation around the circulation center is more important. Considering also that Fig. 6 is a composite, and as Wang (2018) noted, individual genesis cases could exhibit peaks farther or closer to the center, and/or with more or less azimuthal coverage.

4. Pregenesis evolution of precipitation properties

a. Total raining area

Figure 7a shows the evolution of the distributions of 3B42 raining fraction (proxy for total raining area) within 3° of the center for each 24-h period prior to genesis, up to 5 days before TC genesis. All basins are composited together for each period in this figure. Consistent with Fig. 3a, distributions in Fig. 7a indicate that the total raining area in nondeveloping disturbances is significantly less than any day in the pregenesis stage of developing disturbances. Even 96–120 h before genesis, developing disturbances are significantly different (have more total raining area) than nondeveloping disturbances. The other important result from Fig. 7a is that as the pregenesis stage progresses closer to the genesis time, there is an overall increase in the total raining area (e.g., about a 15% increase in the median rainfall coverage in the periods between 96–120 and 0–24 h prior to genesis). Consistent with Fritz et al. (2016) and Wang (2018), this proxy suggests that a trend toward more areal coverage of rainfall around the center may be an indicator that a genesis event could be nearing. In addition, the rain volume appears to increase as genesis nears, as the contribution from the rain rate also shows a

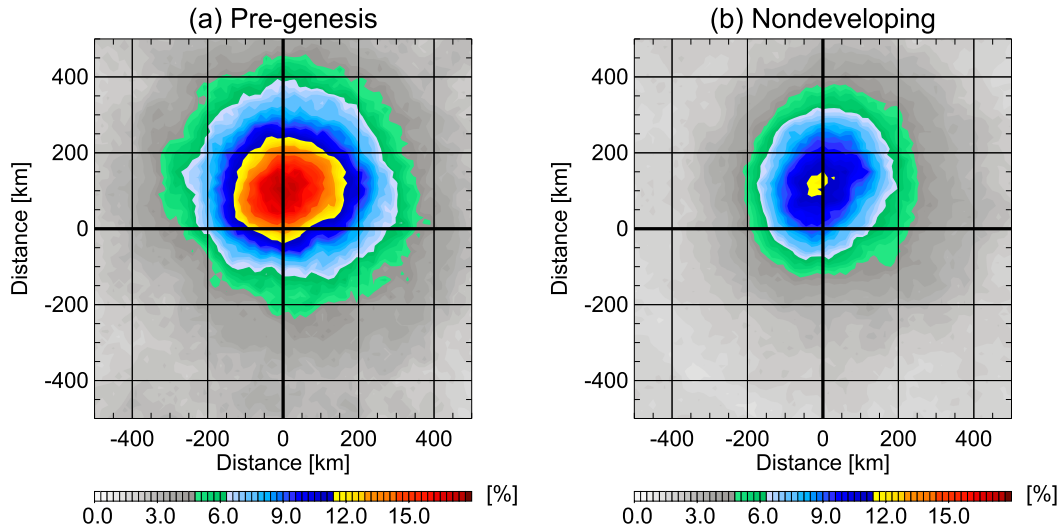


FIG. 6. Fractional occurrence of 85–91-GHz PCT ≤ 250 K for (a) pregenesis and (b) nondeveloping overpasses relative to the 850–200-hPa, or deep-layer, vertical wind shear heading (pointing “up”), such that the upper-right quadrant is DSR, upper-left quadrant is DSL, lower-left quadrant is USL, and lower-right quadrant is USR. Axes are the distance from the center. The number of overpasses contributing within a single grid varies between 4309 and 5352 for pregenesis and between 7029 and 8585 for nondeveloping.

noticeable increase (Fig. 8). As Fig. 8 indicates, there is a trend toward higher conditional mean rain rate as genesis nears, with the 24–48- and 0–24-h periods exhibiting the most distinguishing and highest rain rate distributions. The differences in the distributions from 120 to 24 h prior to genesis also suggest an increasing trend in total precipitating (raining) area for the PMW proxy (i.e., fractional coverage of 85–91-GHz PCT ≤ 250 K) (Fig. 7b). Although not as progressive as the increase observed in the 3B42 raining fraction (Fig. 7a)—the

24–48- and 72–96-h distributions are nearly identical—the period 0–24 h prior to genesis is still significantly greater than any period prior to genesis. Overall, proxies of raining area from two separate datasets (3B42 and PMW) suggest that, at the very least, the pregenesis stage exhibits uniquely larger raining areas within a day of genesis, with at least some increasing trend from 96 to 24 h prior, the degree of which is sensitive to the dataset used.

Given that precipitation characteristics vary between basins (section 3), the observed pregenesis trends in

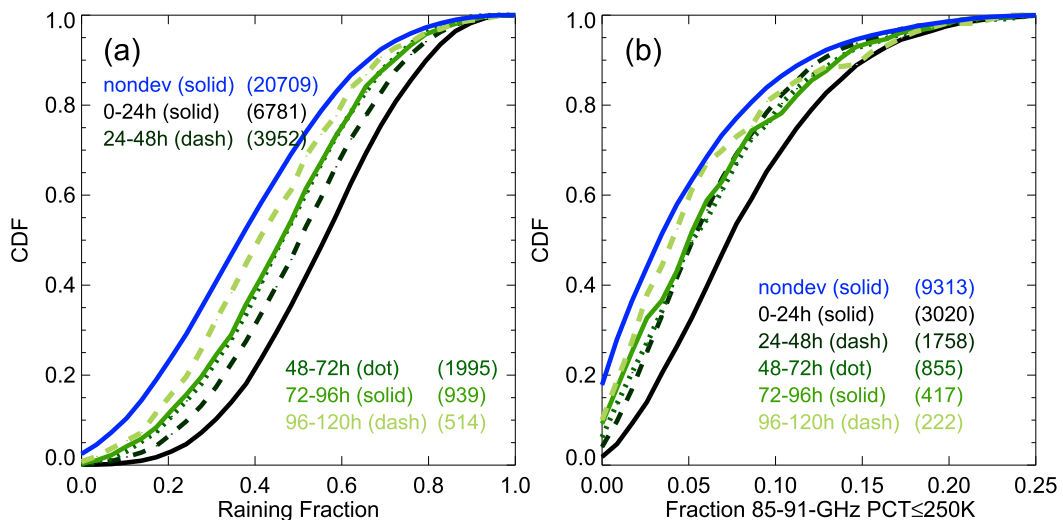


FIG. 7. CDF of (a) raining fraction (3B42 rain rate $> 0.1 \text{ mm h}^{-1}$) and (b) the fractional coverage of 85–91-GHz PCT ≤ 250 K within 3° of the center for the 96–120-, 72–96-, 48–72-, 24–48-, and 0–24-h periods prior to genesis for developing disturbances and for nondeveloping disturbances. Sample sizes are shown in the legend in parentheses.

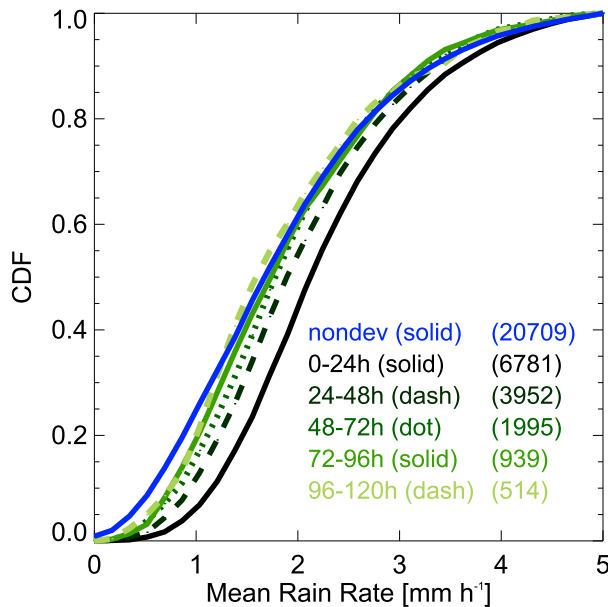


FIG. 8. As in Fig. 7a, but for the CDF of the conditional mean 3B42 rain rate.

Fig. 7 must be analyzed for each basin individually, which is summarized in Fig. 9. In the AL (Figs. 9a,b), the increasing trend in total raining area observed in Fig. 7 is less obvious as the 0–24-h distribution is much closer to the 24–48-, 48–72-, and 72–96-h distributions for each data type (3B42, Fig. 9a; PMW, Fig. 9b). Therefore, the tendency in total raining area appears to be a less useful predictor in that basin. In contrast, the EP/CP (Figs. 9c,d) have significantly higher raining fraction distributions for 0–24-h period (and also 24–48-h period for 3B42, Fig. 9c), which suggests that the trend in areal rainfall coverage—particularly within 48 h of genesis—is a better predictor in the EP/CP. In the WP (Figs. 9e,f), NIO (Figs. 9g,h), SIO (Figs. 9i,j), and SP (Figs. 9k,l), trends are more difficult to identify considering the limitations caused by smaller sample sizes in the periods more than 2 days before genesis. Although results in these basins should not be considered to be as robust as the AL and EP/CP because of those smaller sample sizes, both 3B42 and PMW data at least suggest that similar increasing trends are observed within 48 h of genesis in the WP and SIO. The trend is much less clear in the NIO and SP distributions, but this is not considered a robust result due to the smaller sample sizes in those basins.

b. Areal coverage of deep convection

Figure 10a shows the evolution of the areal coverage of deep convection during the pregenesis stage using the fractional coverage of heavy 3B42 rain rates as a proxy, for all basins composited together. Figure 10a indicates

that the areal coverage of heavy rain (i.e., deep convection) generally increases as genesis nears, with the largest increase observed from 24–48 to 0–24 h prior to genesis. From 48 to 120 h prior to genesis, relatively less daily change is observed in the areal coverage. This indicates that the trend in the areal coverage of deep convection, at least using heavy rain rate as a proxy, could also be a useful predictor of genesis.

Similar to Fig. 10a, 10c, and 10d instead show pregenesis distributions for the areal coverage of deep convection using PMW proxies (fractional coverage of 225 and 210 K PMW PCT). Figure 10c suggests a less distinguishable trend in the areal coverage of deep convection between 48 and 120 h than seen with 3B42 (Fig. 10a), with only the period within a day of genesis having significantly greater deep convective coverage than any day prior. In addition, as the PMW threshold is decreased to 210 K (Fig. 10d; representative of the areal coverage of more intense convection) the differences between the 0–24 h and earlier periods become even less clear, although the fractional coverage at 210 K is also one-half that of 225 K. It is likely that as the PCT threshold is decreased further (i.e., increased convective intensity), the differences between periods in the pregenesis stage will become even more indistinguishable (Fig. 10b). As with the comparison between pregenesis and nondeveloping cases (section 3b, Fig. 5), this result at least suggests, in a composite framework, that the occurrence of more intense, deep convection does not differentiate well developing from nondeveloping cases. Certainly, given the typically low percentage of coverage of more intense convection, case-to-case variability within individual case comparisons between developers and nondevelopers could be larger.

As with the total raining area (Figs. 7, 9), the trend in the areal coverage of deep convection observed in the global composite in Fig. 10 varies some in each basin. The AL (Fig. 11a), EP/CP (Fig. 11c), WP (Fig. 11e), and SIO (Fig. 11i) all appear to contribute to the increasing trend in 3B42 heavy rain rates observed in Fig. 10a, with the WP and SIO exhibiting the most significant differences between 0–24 and 24–48 h. The trend is less clear between 48 and 120 h, particularly in the AL and EP/CP where sample sizes offer more robustness. As before, small samples in the NIO and SP prevent robust conclusions on trends in those basins.

The pregenesis trend in the areal coverage of deep convection using PMW as proxy (Fig. 11, right column), however, is not as consistent as 3B42. Particularly for the AL (Fig. 11b), which exhibits very little difference between any pregenesis period, even within 48 h of genesis. This result appears to differ somewhat from the composite results shown in Wang (2018), Fritz et al. (2016),

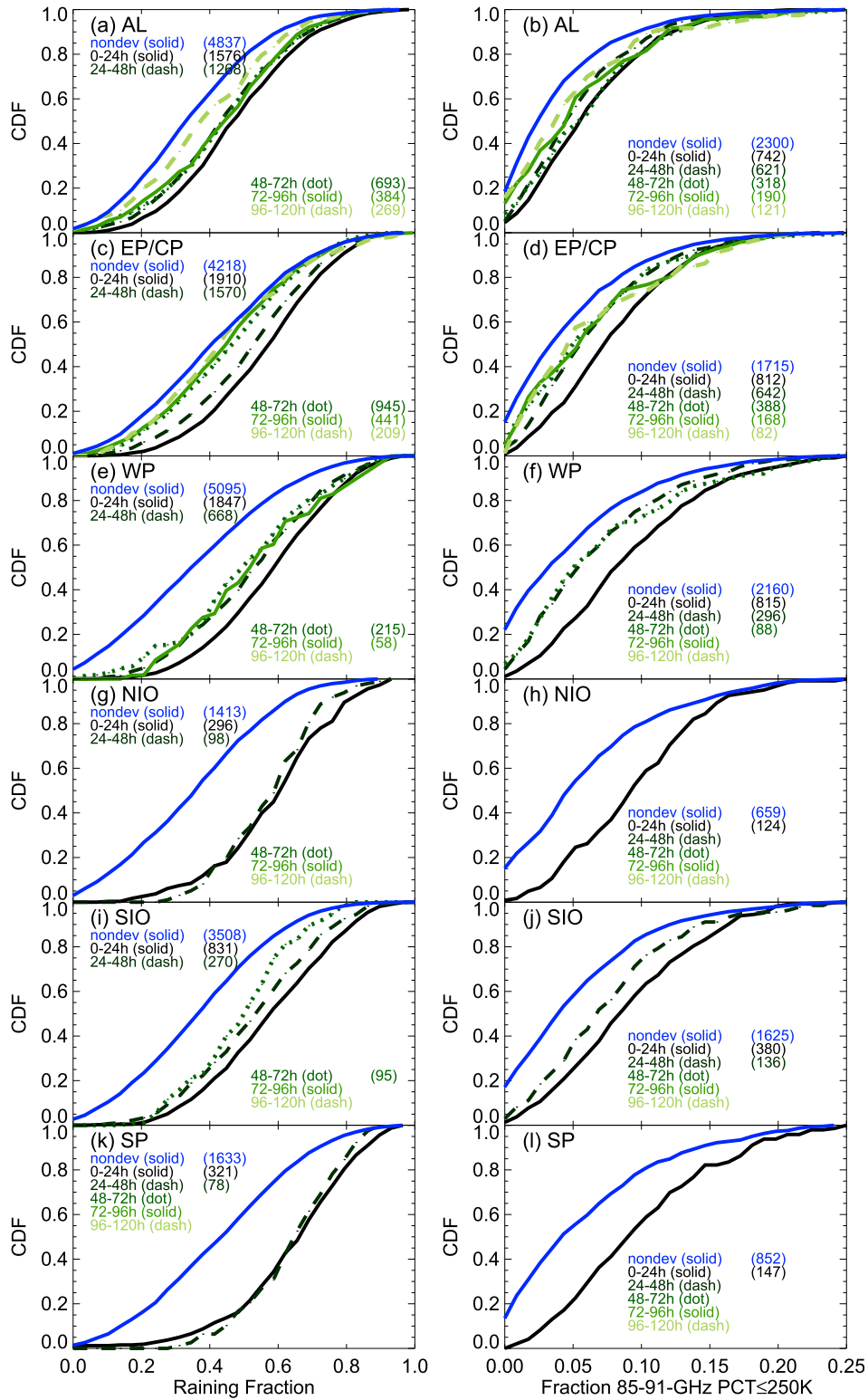


FIG. 9. As in Fig. 7, but separated for each basin: (a),(b) AL, (c),(d) EP/CP, (e),(f) WP, (g),(h) NIO, (i),(j) SIO, and (k),(l) SP. Distributions with less than 50 samples are excluded.

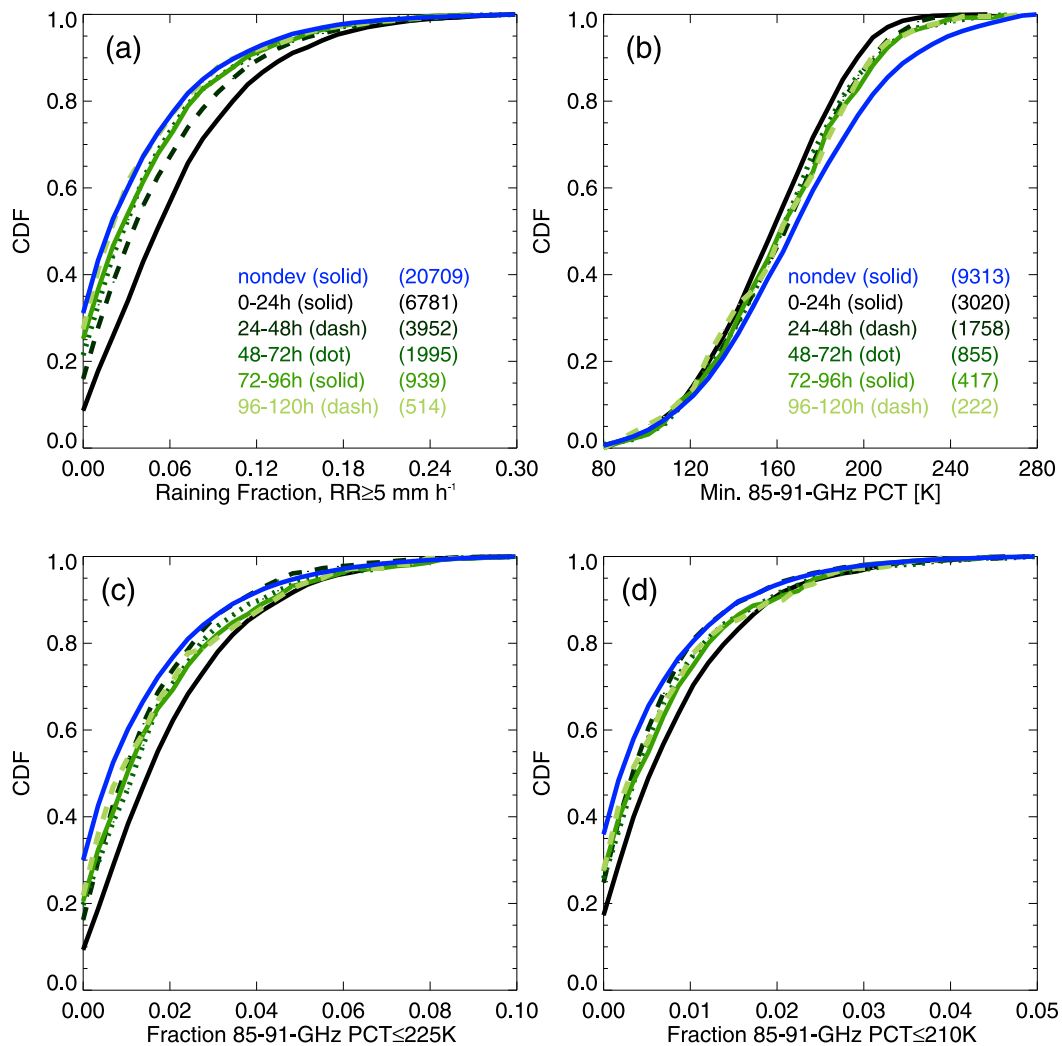


FIG. 10. As in Fig. 7, but for the CDF of (a) the fractional coverage of heavy rain (3B42 rain rate $\geq 5 \text{ mm h}^{-1}$), (b) minimum 85–91-GHz PCT, (c) the fractional coverage of 85–91-GHz PCT $\leq 225 \text{ K}$, and (d) the fractional coverage of 85–91-GHz PCT $\leq 210 \text{ K}$. Sample sizes noted in (b) are the same for (c) and (d).

and Leppert et al. (2013b), all of whom showed increases in the areal coverage of convection within 36–48 h of genesis in AL cases. These apparently differing results between studies, and also between 3B42 and PMW used here, seem to emphasize a sensitivity of this result to data type and the thresholds used to define deep convection. The 210- and 225-K thresholds used for deep convection in this study are likely stronger than the thresholds and proxies used in those other composite studies, and as seen in Fig. 10b, as the PCT threshold is increased (toward thresholding “weaker” convection) the 24-h period before genesis shows an increased difference compared to earlier periods. In addition, 3B42 rain rates are predominantly retrieved from IR data (PMW does contribute, but less often due to its polar orbit) and could alternatively reflect a daily increase in

cloud cover, interpreted by 3B42 to be precipitation. Considering that Wang (2018) and Leppert et al. (2013b) used IR data to threshold areas of “cold cloudiness,” and that IR mainly contributes to the 3B42 rain rate retrieval, there is some consistency between these studies and the observed trend in 3B42 heavy rain fraction (Fig. 11a). Overall, given that PMW frequencies are more directly sensitive to precipitation, the lack of a trend in deep convective coverage in the AL during genesis should be taken with caution, but not necessarily dismissed.

Although cautioned by their smaller sample sizes, it is worth noting that even the 96–120- and 72–96-h, 225- and 210-K distributions are often similar to the 24–48-h distribution (Figs. 10, 11). Therefore, although their fractional coverage may be higher, periods with high

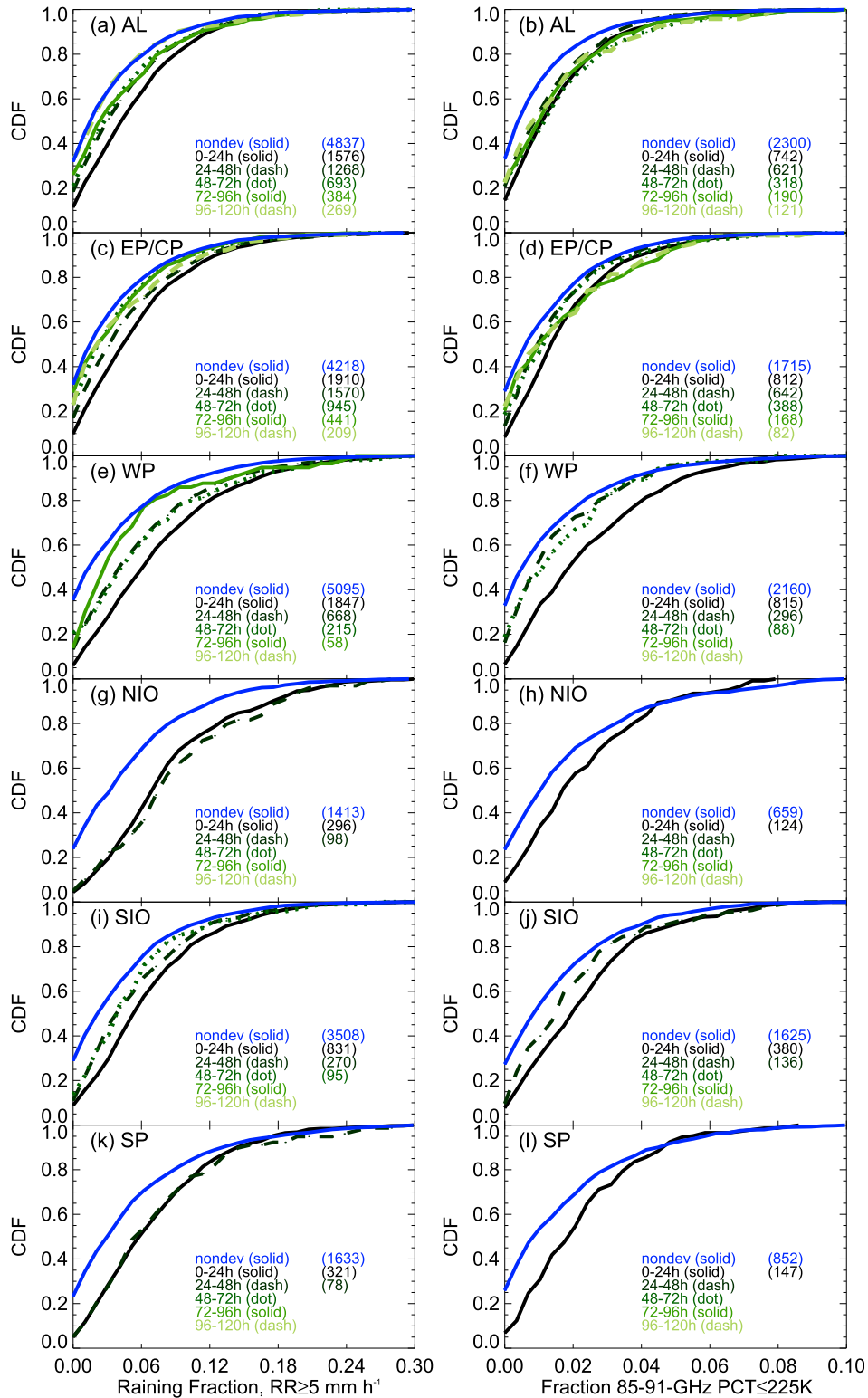


FIG. 11. As in Fig. 9, but showing the fractional coverage of (a),(c),(e),(g),(i),(k) heavy rain (3B42 rain rate $\geq 5 \text{ mm h}^{-1}$) and (b),(d),(f),(h),(j),(l) 85-91-GHz PCT $\leq 225 \text{ K}$.

areal coverage of deep convection (e.g., in organized MCSs) are certainly not exclusive to the period within 48 h of genesis. Although individual MCSs may not directly result in TC genesis, they likely still play a critical role in the development process even 3 or more days before formation (Zehr 1992; Lee et al. 2008; Zawislak and Zipser 2014b). For example, the cumulus congestus, midlevel convection, or stratiform rain contributions to their precipitation could gradually moisten the lower and middle troposphere such that inner core deep convection becomes self-sustaining and low-level spinup is favored (Wang 2014; Fritz et al. 2016).

c. Spatial coverage and proximity of rainfall to the center

Similar to Fig. 6, Fig. 12 shows the percent occurrence of 85–91-GHz PCT ≤ 250 K except separated for the pregenesis life cycle. The most noticeable result from Fig. 12 is the significant increase in precipitation occurrence around the circulation center in all quadrants in the period from 24–48 to 0–24 h prior to genesis. In the days prior, a precipitation increase is less apparent. In addition, the proximity of precipitation (defined by the radial distance of the maximum occurrence) to the center moves somewhat closer to the center as genesis nears (from ~ 150 km for the 48–72-h period to ~ 100 km for the 0–24-h period), and, perhaps more important, there appears to be a consolidation of precipitation in the downshear quadrants. The evolution observed in Fig. 12 is very much consistent with the composite quantified with IR satellite data in Wang (2018). As Wang (2018) concluded, this consolidation could reflect an increased organization of precipitation (convection) around the center, perhaps becoming more organized within larger contiguous precipitating areas. It could also perhaps be an indicator that the developing center itself is becoming more clearly defined within some organized area of precipitation. This organization is also mirrored in the spatial distributions of 210-K occurrence (Fig. 13); the distributions evolve from a more scattered signal 72–96 h prior, to a much more consolidated distribution 24–48 and 0–24 h before genesis. Note that, while this is a pixel-based study, statistics based on defining contiguous precipitation features (PFs) (as used for TCs in Jiang et al. 2011) could better reveal if the increase in raining area also corresponds to more organized, larger contiguous raining areas. Likewise, as in Fig. 6, individual cases within the composite could see much less of an increase in coverage and occurrence during the pregenesis stage, and still develop.

Figure 12 is replicated for each basin individually (not shown) and generally shows that each basin exhibits similar trends as the global composite. Though the magnitude

of the fractional occurrence varies between basins, the trend toward consolidation of precipitation downshear of the developing center each day as genesis nears is ubiquitous across basins. Perhaps interestingly, there is somewhat of a decrease in precipitation observed from the 48–72- to 24–48-h period in the AL (also seen in Fig. 11a). In the AL where longer pregenesis periods are more frequent, this may be a robust result. This brief decrease in precipitation 24–48 h before genesis could be related to the increase in tropospheric stability (due to warming in the mid- to upper troposphere and cooling in the low troposphere) that has been previously noted in observational data (e.g., Raymond et al. 2011; Komaromi 2013; Zawislak and Zipser 2014a), though this is purely speculative.

5. Discussion and conclusions

This study expands upon recent case (Zawislak and Zipser 2014a,b) and composite study (Leppert et al. 2013a,b; Fritz et al. 2016; Wang 2018) evaluations of precipitation properties involved in tropical cyclogenesis by analyzing a multiyear, global database of passive microwave (PMW) overpasses and TRMM 3B42 data of nondeveloping tropical disturbances and the pregenesis stage of developing tropical disturbances. The study quantified precipitation statistics using PMW brightness temperatures as proxies for precipitation in the 85–91-GHz imaging channels of multiple spaceborne sensors (AMSR-E, AMSR2, TMI, GMI, SSM/I, and SSMIS), as well as retrieved rain rates from TRMM 3B42. Proxies mainly focused on the overall raining (precipitating) area, the areal coverage of deep convection, and the azimuthal coverage and radial distance of precipitation to the disturbance (i.e., invest) center (as classified and located by NHC and JTWC). The introduction posed three questions to be answered in this study, and the following summarizes the findings for each question:

a. What precipitation properties most distinguish developing tropical disturbances from nondeveloping disturbances?

The total raining (precipitating) area clearly differentiates disturbances that develop from ones that do not develop, and while the degree to which the total raining area distinguishes developing from nondeveloping tropical disturbances varies by basin, the pregenesis stage ubiquitously exhibits significantly greater total raining area (even as many as 5 days prior to genesis) than nondeveloping disturbances (Figs. 3, 6). Likewise, the conditional mean rain rates in the pregenesis stage are also significantly greater than nondeveloping disturbances in each basin (Fig. 4). Considered in combination with the

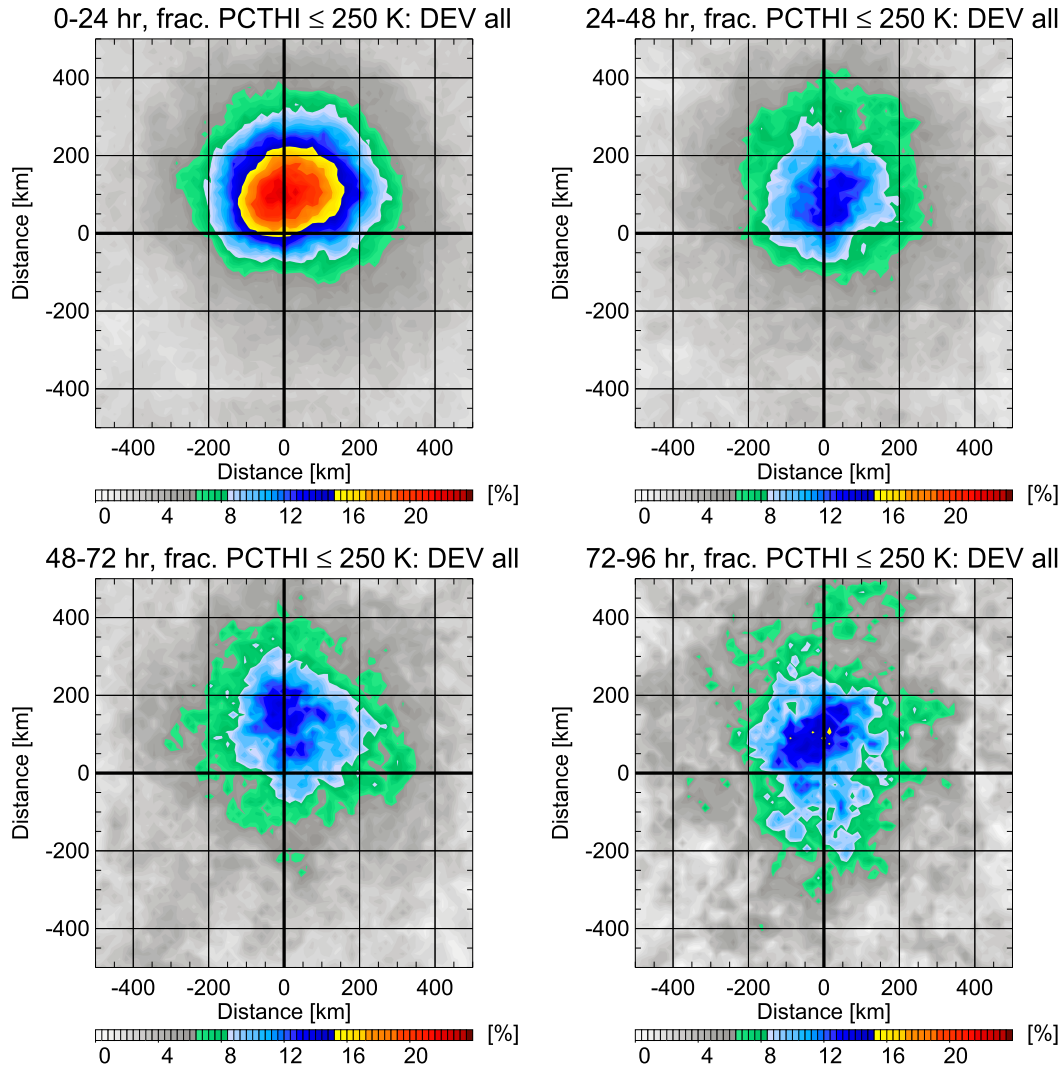


FIG. 12. As in Fig. 6, but showing the fractional occurrence of 85–91-GHz PCT ≤ 250 K for (top left) 0–24, (top right) 24–48, (bottom left) 48–72, and (bottom right) 72–96 h prior to genesis. Sample sizes in the grid vary from 2038 to 2515 for the 0–24-h period, from 1175 to 1462 for the 24–48-h period, from 564 to 715 for the 48–72-h period, and from 269 to 350 for the 72–96-h period.

larger raining area, the total rain volume (amount of precipitation falling around the center) is subsequently also greater for developing cases and should be considered *one of the most useful precipitation-related predictors for TC genesis*. As for the spatial distribution, having precipitation closer to the center should be considered a favorable condition for genesis to occur. However, since the radial proximity of the peak to the center in the pregenesis composite is similar to the nondeveloping composite (Fig. 6), and likely varies greatly from case to case, it is hypothesized that close proximity (~ 100 km) of precipitation is favorable, but not sufficient alone, for genesis. Pregenesis tropical disturbances do, however, exhibit greater precipitation

coverage azimuthally around the center as compared to nondeveloping disturbances, which reinforces the importance of not only having greater total raining area, but also having greater coverage around the circulation center.

Multiple proxies were used to analyze the areal coverage of deep convection: heavy 3B42 rain rates (≥ 5 mm h^{-1}), as well as 85–91-GHz PMW PCT ≤ 225 and 210 K. Overall, the areal coverage of deep convection is significantly greater during the pregenesis stage of developing disturbances compared to nondeveloping disturbances (Figs. 5a,c,d). However, as the threshold convective intensity increases (decreasing PCT, Fig. 5b), the occurrence, and likely areal coverage, of deep convection appears to become a less useful

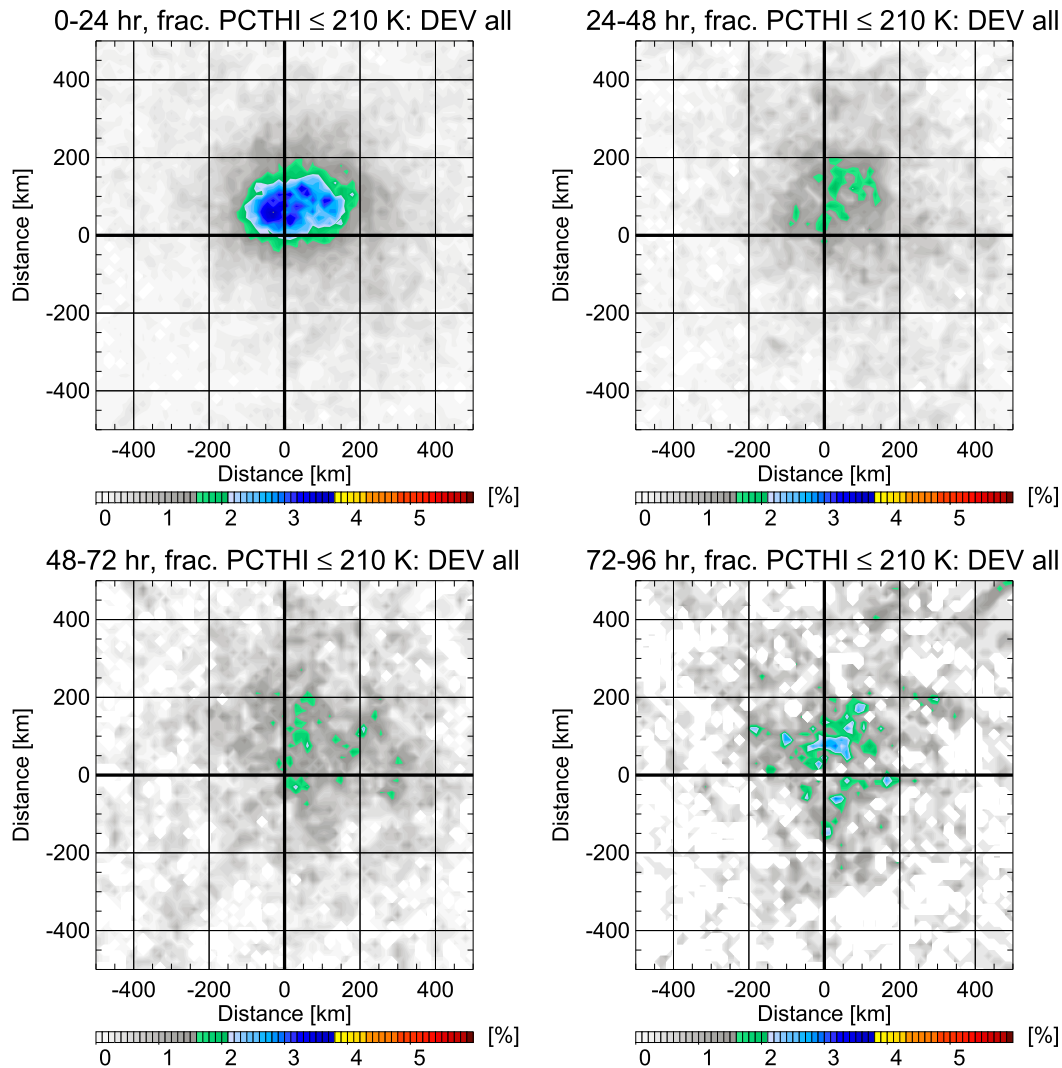


FIG. 13. As in Fig. 12, but showing the fractional occurrence of 85–91-GHz PCT \leq 210 K.

predictor for genesis since the differences between the pregenesis and nondeveloping distributions become less distinguishable. This result suggests that while the areal coverage of deep convection is likely an important distinguisher of developing cases, as more intense convection is considered (defined by low PCTs: <210 K) its occurrence and coverage likely become less unique in developing tropical disturbances. This should not be interpreted that more intense, deep convection is not important for genesis, just that it may not be the most useful predictor for separating developing from nondeveloping disturbances.

In this study, the “usefulness” of genesis predictors are concluded based on the composite results, and may not necessarily apply well to genesis prediction for individual cases. Comparisons of precipitation between individual developing and nondeveloping cases could

vary greatly from the composite differences and tendencies shown in this study (e.g., an individual nondeveloping disturbance within this case sample could certainly exhibit greater convective area than other developing cases), especially considering the stochastic nature of convection (Wang 2018). That being said, the precursor to this study (Zawislak and Zipser 2014a,b) analyzed, individually, 12 developing and 3 nondeveloping Atlantic tropical disturbances using identical proxies. The composite results shown here, supporting the importance of total raining area as a predictor for TC genesis, are consistent with those individual case results. As they also used satellite proxies of precipitation properties in a composite framework, the results presented here can also be reasonably compared against those in Leppert et al. (2013a,b), who analyzed precipitation differences between developing and nondeveloping easterly waves in the AL and EP.

Leppert et al. (2013a,b) used the coverage of cold IR cloud tops (brightness temperatures ≤ 210 K and ≤ 240 K) to find that the coverage of convection most distinguished developing from nondeveloping easterly waves in both the AL and EP. The analogous proxies used in this study—the fractional coverage of 3B42 heavy rain rates (≥ 5 mm h⁻¹) and 85–91-GHz PCT ≤ 225 K and ≤ 210 K—agree with this result. Leppert et al. (2013b) also found that predictors for the intensity of convection (they used lightning flash rate, mean PCT for 85-GHz pixels ≤ 200 K, mean PCT for 37-GHz pixels ≤ 260 K, and reflectivity profiles) were less important to genesis than the coverage of convection, and results shown in this study for the minimum PCT agree with this conclusion.

b. How do the precipitation properties of developing versus nondeveloping tropical disturbances vary between different ocean basins?

The most obvious difference in precipitation properties among all basins is the total raining area. The NIO, SIO, SP, and WP exhibit the largest total raining areas in the pregenesis stage, while the AL and EP/CP exhibit distinguishably less raining area (Fig. 3). The degree of difference between pregenesis and nondeveloping tropical disturbances raining areas also vary between each basin; for example, the difference in the total raining area is much greater in the NIO, SIO, SP, and WP than in the AL and EP/CP (Fig. 3). *This suggests that the total raining area could be a better predictor of the genesis fate of disturbances in the NIO, SIO, SP, and WP, while in the AL and EP/CP it is somewhat more challenging to predict genesis using the total raining area metric alone.*

The results for the areal coverage of deep convection that are presented for the basin separation (Fig. 5) are generally consistent with the total raining area. In nearly all basins, and in both the 3B42 and PMW proxies, there is significantly greater areal coverage of deep convection in the pregenesis stage as compared to nondeveloping disturbances, which suggests that *the areal coverage of deep convection is also an adequate proxy to distinguish developing from nondeveloping disturbances in all basins.* Similar to the total raining area, the AL and EP/CP exhibited the least coverage of deep convection of all basins, with the differences between developing/nondeveloping generally greater for the WP, SIO, SP, and NIO than in the AL and EP/CP (Fig. 5).

c. How do various precipitation properties evolve both spatially and temporally during the pregenesis stage of developing disturbances?

Although the increasing trend in the PMW proxy of total raining area (Fig. 7b) is not as progressive as the

increasing trend observed in the 3B42 proxy (Fig. 7a), results for both proxies indicate that the total raining area increases during the pregenesis stage, particularly within the last 48 h before genesis. In addition, there is a progressive increase in the conditional mean 3B42 rain rate preferentially within that same period (Fig. 8). *This suggests that an increasing trend in total raining area and the total rain volume around the circulation center could be useful predictors for TC genesis.* The precipitation in the 0–24-h period prior to genesis was particularly unique compared to the previous days, exhibiting a clear increase in occurrence and consolidation (and likely organization) over a large area around the center (Fig. 12). Although other composite studies were limited to the AL and EP basins, these noteworthy results are generally consistent with the other satellite-based composite studies (Leppert et al. 2013a,b; Wang and Hanks 2016; Fritz et al. 2016; Wang 2018). Wang (2018) concluded for AL cases that the increase in convective area and convective intensity around the center enhances the radial gradient of heating and drives the transverse circulation that concentrates low-level vorticity, and that convective organization around the center is thus a key feature of TC genesis. Results shown in this study support that conclusion for not only the AL, but the other basins as well.

In comparison with composite results shown in this study, however, the 12 individual AL case studies in Zawislak and Zipser (2014b) did not show a particularly noticeable increasing trend, or a uniquely larger total raining area within a day of genesis. Although the composite for all basins indicates a more obvious trend (Fig. 7), the subset for the AL (Figs. 9a,b) actually exhibited the least distinguishable trend among all of the basins (with larger sample sizes), suggesting that the individual case results in Zawislak and Zipser (2014b) could be robust in a larger sample. Alternatively, it could reflect that the total raining area in developing cases is more varied in the AL, a conclusion consistent with the cluster analysis presented in Wang (2018), who showed one particular developing cluster (cf. their “cluster 2”) with distinguishably smaller convective systems.

An increasing trend in the areal coverage of deep convection within a day of genesis was also observed in both 3B42 heavy rain area (Fig. 10a), and to a lesser degree in the PMW (Figs. 10c,d) proxies composited for all basins. Similar to the pregenesis and nondeveloping comparison, as lower PCTs associated with more intense convection were considered, differences between periods within the pregenesis stage were less distinguishable. As for the individual basin composites (Fig. 11), while 3B42 and PMW proxies generally both exhibited

some consistency with the global composite (Fig. 10)—at least for the basins where sample size was not as limiting more than 72 h before genesis (as it was for NIO and SP)—the AL stood out as a particularly noticeable example of where the PMW (Fig. 11b) deviated greatly from the trend observed in 3B42 heavy rain (Fig. 11a). In fact, in the AL the fractional occurrence of precipitation and deep convection appear to decrease somewhat from the 48–72 to the 24–48-h period. Having little to no increasing trend in the areal coverage of deep convection in the AL, as seen in the PMW proxy of deep convective coverage, is contrary to the results from the other composite studies (Leppert et al. 2013b; Fritz et al. 2016; Wang 2018). Given that more intense thresholds for deep convection are being used in this study (compared to the other composite studies) and that PMW frequencies are more directly sensitive to precipitation, the lack of a trend in deep convective coverage in the AL should be cautioned, but not necessarily be dismissed. Leppert et al. (2013a,b) and Wang (2018) used IR “cold cloud” coverage as a proxy for deep convection, and it seems plausible that trends in cold cloudiness could differ from the actual precipitating area produced from those clouds.

Consistent with previous work (Zehr 1992; Lee et al. 2008; Zawislak and Zipser 2014b), periods with higher areal coverage of deep convection (e.g., “convective bursts”) are certainly not exclusive to the period within a day of genesis and, although those do not directly result in tropical depression formation, likely still play a critical role in TC genesis even 3 or more days out. Some of the critical aspects in TC genesis, as surmised from modeling (Wang 2012, 2014; Zhang and Zhu 2012) and observational studies (Raymond et al. 2011; Raymond and López Carrillo 2011; Davis and Ahijevych 2012; Komaromi 2013; Zawislak and Zipser 2014a), are the strengthening of a midlevel vortex, favorable preconditioning from moistening (saturation) of the low- to middle troposphere around that vortex, and the development of an upper-level warm core—convective bursts, and the various precipitation modes (i.e., stratiform and convection) that make up those bursts, can favorably contribute in all these aspects.

As stated in Fritz et al. (2016), multiple precipitation modes, such as stratiform rain, as well as congestus convection, contribute to TC genesis, with those related to moderately deep convection being perhaps most critical for preconditioning given that they cover a larger area of the disturbance. Though the various precipitation modes classified in Fritz et al. (2016), particularly stratiform rain and shallow and moderately deep congestus, cannot be separated with the data types used in this study, the increasing trend in total raining area still lends some support to the important relationship

between moistening and precipitation in TC genesis, since it is likely that other precipitation modes, besides deep convection, predominantly contribute to the total raining area presented here. Given the observed increase in raining area, and that the deep convective coverage is largest near the genesis time, this study also reinforces the hypothesis that both top-down and bottom-up development pathways, and their accompanying deep-tropospheric latent heat profiles and spinup mechanisms, likely play a role in the genesis process. While intense, deep convection (e.g., VHTs; Hendricks et al. 2004; Montgomery et al. 2006) was shown to not be unique to developing disturbances when compared to nondeveloping cases, it certainly still could play an important role in the genesis process. In fact, considering how small the 210 K areal fractions are (<5% of the area within 3°) even what would appear to be a small increase in fractional coverage could influence greatly on the vortex development. It is just important to note that the low fractional coverage of deep convection compared to the total precipitating area reinforces the need to look at all precipitation modes during genesis, as emphasized in Fritz et al. (2016).

Overall, this study has uniquely highlighted that precipitation properties during tropical cyclogenesis can differ greatly in various ocean basins around the globe, which is indicative of varying dynamic and thermodynamic background conditions. For example, smaller overall raining and deep convective fractions in both developing and nondeveloping tropical disturbances were observed in the AL than in the WP, which suggests that the background environment is likely more favorable (i.e., higher overall tropospheric humidity, higher SST, and enhanced low-level convergence) for more widespread precipitation in the WP.

It also motivates an interesting question: *is less precipitation required to develop a storm in the AL than in the WP?* Albeit a simplified, and certainly speculative, hypothesis, the basin differences could reflect that “preexisting disturbances” in the AL [e.g., African easterly waves (AEWs)] are typically more dynamically favorable for genesis (e.g., having strong vorticity in the middle troposphere) than those in the WP, which tend to originate in monsoonal shear, confluence, and gyre regions (e.g., Holland 1995; Harr et al. 1996; Ritchie and Holland 1999; Harr and Chan 2005). Fu et al. (2012) and Peng et al. (2012) offer strong support for this hypothesis as they concluded that thermodynamic variables play a dominant role in controlling the genesis of AEWs in the AL (Peng et al. 2012), given that AEWs are already dynamically more favorable for genesis, while genesis in the WP is more sensitive to dynamic factors, given that

thermodynamic variables differ less between developing and nondeveloping disturbances (Fu et al. 2012). Recall that studies have suggested that low-level vortex intensification is favored when a coherent, midtropospheric vortex in a near-saturated environment exists (Nolan 2007; Raymond and López Carrillo 2011; Raymond et al. 2011; Wang 2012). AEWs inherently provide that coherent midlevel circulation, but must overcome potentially unfavorable tropospheric moisture and humidity, while monsoon troughs are generally more thermodynamically favorable and coherent in the low levels, but require MCVs (originating from MCSs) to develop a coherent midtropospheric vortex. Although Wang (2018) only analyzed Atlantic genesis cases, results from their cluster analysis are also consistent with this hypothesis as their “cluster 2” revealed that TC genesis can occur despite characteristically weaker convection, that covers less area, due to less than favorable environmental humidity. A follow-up study will further investigate the link between the observed PMW satellite data and proxy precipitation properties for tropical disturbances shown here in each basin and the environmental properties associated with development and nondevelopment of those disturbances.

Acknowledgments. This study is funded by the NASA New (Early Career) Investigator Program in Earth Science, Grant NNX16AH55G, under the direction of Dr. Allison Leidner (formerly Dr. Lin Chambers). The author acknowledges George R. Alvey III and Dr. Ed Zipser at the University of Utah, Dr. Chuntao Liu at Texas A&M Corpus Christi, as well as Drs. Yongxian Pei and Haiyan Jiang at Florida International University, for their assistance in the development of the dataset and interpretation of the results; Drs. Jason Dunion and Ghassan Alaka (of the University of Miami/CIMAS and NOAA/AOML/Hurricane Research Division), as well as three anonymous reviewers, contributed valuable comments and suggestions that improved the paper.

REFERENCES

- Alvey, G. R., III, J. Zawislak, and E. Zipser, 2015: Precipitation properties observed during tropical cyclone intensity change. *Mon. Wea. Rev.*, **143**, 4476–4492, <https://doi.org/10.1175/MWR-D-15-0065.1>.
- Ashcroft, P., and F. J. Wentz, 2013: AMSR-E/Aqua L2A global swath spatially-resampled brightness temperatures, version 3. NASA National Snow and Ice Data Center Distributed Active Archive Center, accessed 17 April 2017, https://doi.org/10.5067/AMSR-E/AE_L2A.003.
- Berg, W., and Coauthors, 2016: Intercalibration of the GPM microwave radiometer constellation. *J. Atmos. Oceanic Technol.*, **33**, 2639–2654, <https://doi.org/10.1175/JTECH-D-16-0100.1>.
- Davis, C. A., and D. A. Ahijevych, 2012: Mesoscale structural evolution of three tropical weather systems observed during PREDICT. *J. Atmos. Sci.*, **69**, 1284–1305, <https://doi.org/10.1175/JAS-D-11-0225.1>.
- Fritz, C., Z. Wang, S. W. Nesbitt, and T. J. Dunkerton, 2016: Vertical structure and contribution of different types of precipitation during Atlantic tropical cyclone formation as revealed by TRMM PR. *Geophys. Res. Lett.*, **43**, 894–901, <https://doi.org/10.1002/2015GL067122>.
- Fu, B., M. S. Peng, T. Li, and D. E. Stevens, 2012: Developing versus nondeveloping disturbances for tropical cyclone formation. Part II: Western North Pacific. *Mon. Wea. Rev.*, **140**, 1067–1080, <https://doi.org/10.1175/2011MWR3618.1>.
- Harr, P. A., and J. Chan, 2005: Monsoon impacts on tropical cyclone variability. *The Global Monsoon System: Research and Forecast*, C.-P. Chang, B. Wang, and N.-C. G. Lau, Eds., World Meteorological Organization, 512–542.
- , M. S. Kalafsky, and R. L. Elsberry, 1996: Environmental conditions prior to formation of a midlevel tropical cyclone during TCM-93. *Mon. Wea. Rev.*, **124**, 1693–1710, [https://doi.org/10.1175/1520-0493\(1996\)124<1693:ECPTFO>2.0.CO;2](https://doi.org/10.1175/1520-0493(1996)124<1693:ECPTFO>2.0.CO;2).
- Hendricks, E. A., M. T. Montgomery, and C. A. Davis, 2004: The role of “vortical” hot towers in the formation of Tropical Cyclone Diana (1984). *J. Atmos. Sci.*, **61**, 1209–1232, [https://doi.org/10.1175/1520-0469\(2004\)061<1209:TROVHT>2.0.CO;2](https://doi.org/10.1175/1520-0469(2004)061<1209:TROVHT>2.0.CO;2).
- Holland, G. J., 1995: Scale interaction in the western Pacific monsoon. *Meteor. Atmos. Phys.*, **56**, 57–79, <https://doi.org/10.1007/BF01022521>.
- Huffman, G. J., and Coauthors, 2007: The TRMM Multisatellite Precipitation Analysis (TMPA): Quasi-global, multiyear, combined-sensor precipitation estimates at fine scales. *J. Hydrometeorol.*, **8**, 38–55, <https://doi.org/10.1175/JHM560.1>.
- Jiang, H., C. Liu, and E. J. Zipser, 2011: A TRMM-based tropical cyclone cloud and precipitation feature database. *J. Appl. Meteor. Climatol.*, **50**, 1255–1274, <https://doi.org/10.1175/2011JAMC2662.1>.
- Kerns, B. K., and E. Zipser, 2009: Four years of tropical ERA-40 vorticity maxima tracks. Part II: Differences between developing and nondeveloping disturbances. *Mon. Wea. Rev.*, **137**, 2576–2591, <https://doi.org/10.1175/2008MWR2545.1>.
- , K. G. Greene, and E. Zipser, 2008: Four years of tropical ERA-40 vorticity maxima tracks. Part I: Climatology and vertical vorticity structure. *Mon. Wea. Rev.*, **136**, 4301–4319, <https://doi.org/10.1175/2008MWR2390.1>.
- Klotzbach, P. J., 2014: The Madden–Julian oscillation’s impacts on worldwide tropical cyclone activity. *J. Climate*, **27**, 2317–2330, <https://doi.org/10.1175/JCLI-D-13-00483.1>.
- Komaromi, W. A., 2013: An investigation of composite dropsonde profiles for developing and nondeveloping tropical waves during the 2010 PREDICT field campaign. *J. Atmos. Sci.*, **70**, 542–558, <https://doi.org/10.1175/JAS-D-12-052.1>.
- Lee, C., K. K. Cheung, J. S. Hui, and R. L. Elsberry, 2008: Mesoscale features associated with tropical cyclone formations in the western North Pacific. *Mon. Wea. Rev.*, **136**, 2006–2022, <https://doi.org/10.1175/2007MWR2267.1>.
- Leppert, K. D., W. A. Petersen, and D. J. Cecil, 2013a: Electrically active convection in tropical easterly waves and implications for tropical cyclogenesis in the Atlantic and east Pacific. *Mon. Wea. Rev.*, **141**, 542–556, <https://doi.org/10.1175/MWR-D-12-00174.1>.
- , D. J. Cecil, and W. A. Petersen, 2013b: Relation between tropical easterly waves, convection, and tropical cyclogenesis: A Lagrangian perspective. *Mon. Wea. Rev.*, **141**, 2649–2668, <https://doi.org/10.1175/MWR-D-12-00217.1>.

- Liu, C., E. J. Zipser, D. J. Cecil, S. W. Nesbitt, and S. Sherwood, 2008: A cloud and precipitation feature database from nine years of TRMM observations. *J. Appl. Meteor. Climatol.*, **47**, 2712–2728, <https://doi.org/10.1175/2008JAMC1890.1>.
- Mohr, K. I., and E. J. Zipser, 1996: Defining mesoscale convective systems by their 85-GHz ice-scattering signatures. *Bull. Amer. Meteor. Soc.*, **77**, 1179–1189, [https://doi.org/10.1175/1520-0477\(1996\)077%3C1179:DMCSBT%3E2.0.CO;2](https://doi.org/10.1175/1520-0477(1996)077%3C1179:DMCSBT%3E2.0.CO;2).
- Montgomery, M. T., M. E. Nicholls, T. A. Cram, and A. B. Saunders, 2006: A vortical hot tower route to tropical cyclogenesis. *J. Atmos. Sci.*, **63**, 355–386, <https://doi.org/10.1175/JAS3604.1>.
- Nolan, D., 2007: What is the trigger for tropical cyclogenesis? *Aust. Meteor. Mag.*, **56**, 241–266.
- Peng, M. S., B. Fu, T. Li, and D. E. Stevens, 2012: Developing versus nondeveloping disturbances for tropical cyclone formation. Part I: North Atlantic. *Mon. Wea. Rev.*, **140**, 1047–1066, <https://doi.org/10.1175/2011MWR3617.1>.
- Raymond, D. J., and S. L. Sessions, 2007: Evolution of convection during tropical cyclogenesis. *Geophys. Res. Lett.*, **34**, L06811, <https://doi.org/10.1029/2006GL028607>.
- , and C. López Carrillo, 2011: The vorticity budget of developing Typhoon Nuri (2008). *Atmos. Chem. Phys.*, **11**, 147–163, <https://doi.org/10.5194/acp-11-147-2011>.
- , S. L. Sessions, and C. López Carrillo, 2011: Thermodynamics of tropical cyclogenesis in the northwest Pacific. *J. Geophys. Res.*, **116**, D18101, <https://doi.org/10.1029/2011JD015624>.
- Ritchie, E. A., and G. J. Holland, 1997: Scale interactions during the formation of Typhoon Irving. *Mon. Wea. Rev.*, **125**, 1377–1396, [https://doi.org/10.1175/1520-0493\(1997\)125<1377:SIDTFO>2.0.CO;2](https://doi.org/10.1175/1520-0493(1997)125<1377:SIDTFO>2.0.CO;2).
- , and —, 1999: Large-scale patterns associated with tropical cyclogenesis in the western Pacific. *Mon. Wea. Rev.*, **127**, 2027–2043, [https://doi.org/10.1175/1520-0493\(1999\)127<2027:LSPAWT>2.0.CO;2](https://doi.org/10.1175/1520-0493(1999)127<2027:LSPAWT>2.0.CO;2).
- Sapiano, M., W. Berg, D. McKague, and C. Kummerow, 2013: Towards an intercalibrated fundamental climate data record of the SSM/I sensors. *IEEE Trans. Geosci. Remote Sens.*, **51**, 1492–1503, <https://doi.org/10.1109/TGRS.2012.2206601>.
- Simpson, J., E. Ritchie, G. J. Holland, J. Halverson, and S. Stewart, 1997: Mesoscale interactions in tropical cyclone genesis. *Mon. Wea. Rev.*, **125**, 2643–2661, [https://doi.org/10.1175/1520-0493\(1997\)125<2643:MIITCG>2.0.CO;2](https://doi.org/10.1175/1520-0493(1997)125<2643:MIITCG>2.0.CO;2).
- Spencer, R. W., H. M. Goodman, and R. E. Hood, 1989: Precipitation retrieval over land and ocean with the SSM/I: Identification and characteristics of the scattering signal. *J. Atmos. Oceanic Technol.*, **6**, 254–273, [https://doi.org/10.1175/1520-0426\(1989\)006<0254:PROLAO>2.0.CO;2](https://doi.org/10.1175/1520-0426(1989)006<0254:PROLAO>2.0.CO;2).
- Tao, C., and H. Jiang, 2015: Distributions of shallow to very deep precipitation – convection in rapidly intensifying tropical cyclones. *J. Climate*, **28**, 8791–8824, <https://doi.org/10.1175/JCLI-D-14-00448.1>.
- , —, and J. Zawislak, 2017: The relative importance of stratiform and convective rainfall in rapidly intensifying tropical cyclones. *Mon. Wea. Rev.*, **145**, 795–809, <https://doi.org/10.1175/MWR-D-16-0316.1>.
- Wang, Z., 2012: Thermodynamic aspects of tropical cyclone formation. *J. Atmos. Sci.*, **69**, 2433–2451, <https://doi.org/10.1175/JAS-D-11-0298.1>.
- , 2014: Role of cumulus congestus in tropical cyclone formation in a high-resolution numerical model simulation. *J. Atmos. Sci.*, **71**, 1681–1700, <https://doi.org/10.1175/JAS-D-13-0257.1>.
- , 2018: What is the key feature of convection leading up to tropical cyclone formation? *J. Atmos. Sci.*, **75**, 1609–1629, <https://doi.org/10.1175/JAS-D-17-0131.1>.
- , and I. Hanks, 2016: Moisture and precipitation evolution during tropical cyclone formation as revealed by the SSM/I–SSMIS retrievals. *J. Atmos. Sci.*, **73**, 2773–2781, <https://doi.org/10.1175/JAS-D-15-0306.1>.
- Zawislak, J., and E. J. Zipser, 2010: Observations of seven African easterly waves in the east Atlantic during 2006. *J. Atmos. Sci.*, **67**, 26–43, <https://doi.org/10.1175/2009JAS3118.1>.
- , and —, 2014a: Analysis of the thermodynamic properties of developing and nondeveloping tropical disturbances using a comprehensive dropsonde dataset. *Mon. Wea. Rev.*, **142**, 1250–1264, <https://doi.org/10.1175/MWR-D-13-00253.1>.
- , and —, 2014b: A multisatellite investigation of the convective properties of developing and nondeveloping tropical disturbances. *Mon. Wea. Rev.*, **142**, 4624–4645, <https://doi.org/10.1175/MWR-D-14-00028.1>.
- Zehr, R. M., 1992: Tropical cyclogenesis in the western North Pacific. NOAA Tech. Rep. NESDIS 61, 181 pp.
- Zhang, D.-L., and L. Zhu, 2012: Roles of upper-level processes in tropical cyclogenesis. *Geophys. Res. Lett.*, **39**, L17804, <https://doi.org/10.1029/2012GL053140>.